地球流体力学（GFD）
オンラインセミナー
2021年11月16日

太陽対流層内部のロスビー波と傾圧不安定波

Rossby waves and baroclinic waves in the Sun’s convection zone

戸次宥人（マックス・プランク太陽系研究所）

共同研究者： Robert Cameron, Laurent Gizon, 他

Interior of the Sun and Helioseismology

- The Sun consists of **radiation zone** (stable / inner 70%) and **convection zone** (unstable / outer 30%)
- Historically, **acoustic (p) modes** and **gravity (g) modes** have been extensively used to probe the interior
- Recently, lots of **inertial modes** have been newly observed on the Sun, including **Rossby waves**
- They are expected to be used as an alternative tool to further probe the interior [Gizon et al. 2021, A&A Letters]

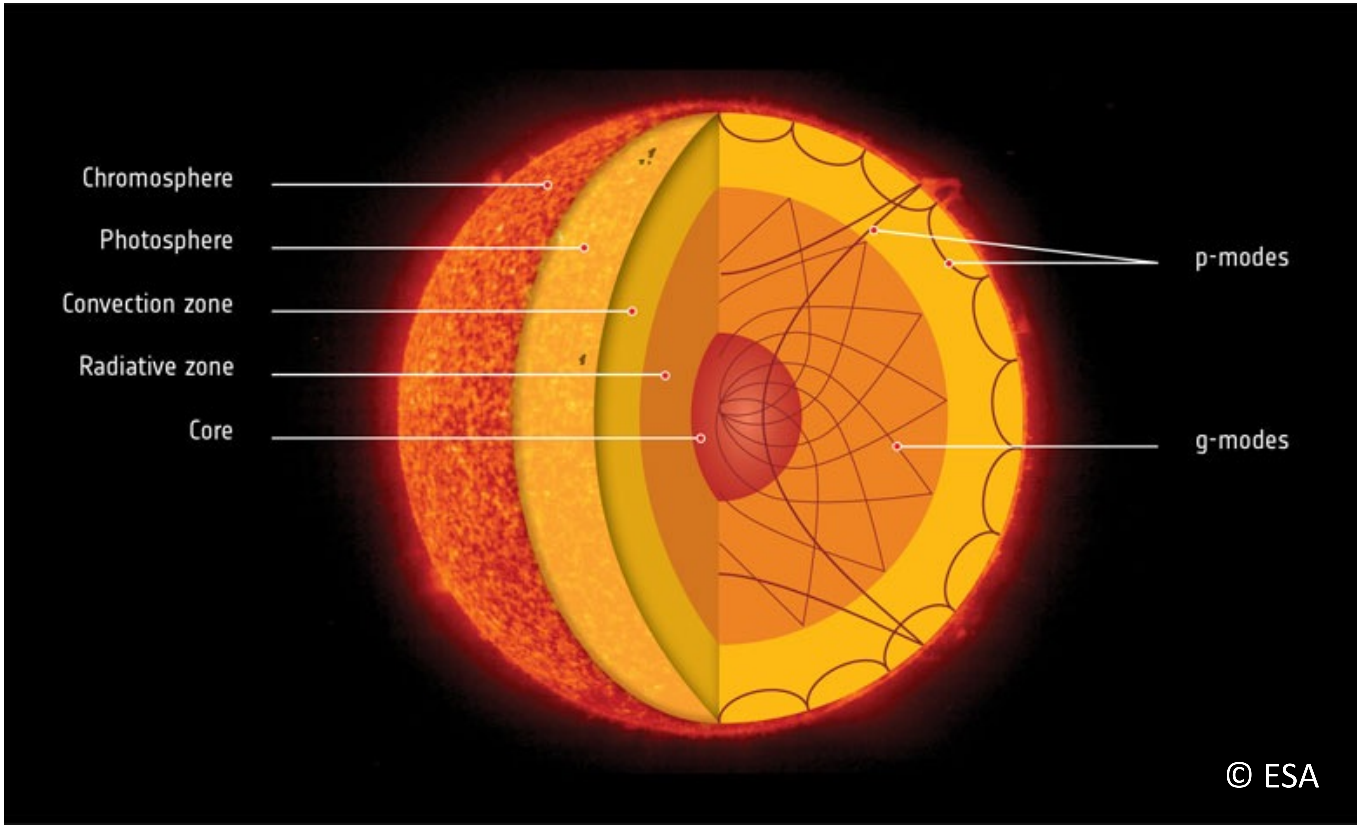

© ESA

What are Rossby waves?

- Rossby waves are global-scale vorticity waves in a rotating fluid that are rooted in the conservation law of potential vorticity Π

$$\frac{D\Pi}{Dt} = 0, \qquad \Pi = \frac{(\zeta + 2\Omega_0) \cdot \nabla S}{\rho}$$

- Rossby waves can be classified based on the so-called β-effects (restoring "force" of Rossby waves)

- A propagation direction of Rossby waves is determined by the sign of β-effect (regardless of its physical origin)

vorticity equation

$$\frac{\partial \zeta_i}{\partial t} = \beta v_j,$$

propagation direct

$$\boldsymbol{s} = \beta \boldsymbol{e}_j \times \boldsymbol{e}_i.$$

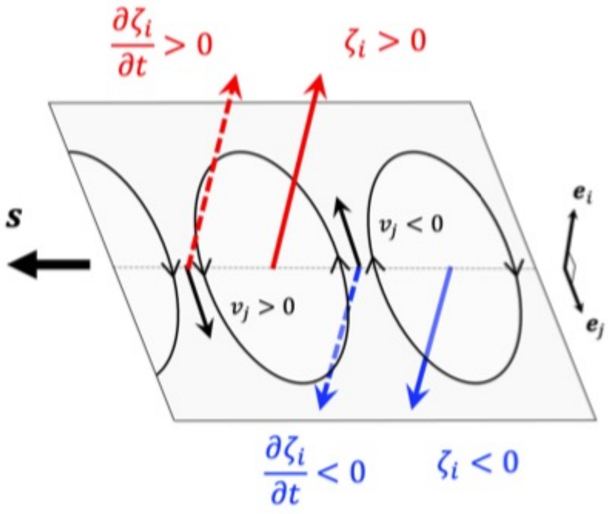

Classification of Rossby waves in the Sun

(traditional) Rossby wave
(r-modes)

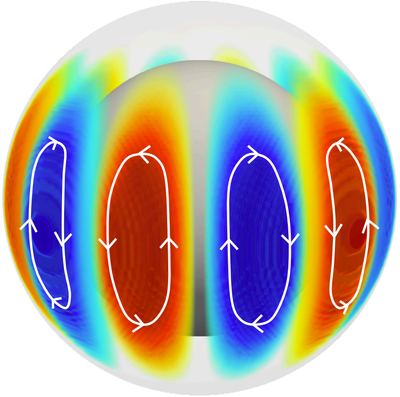

$$\begin{cases} \dfrac{\partial \zeta_r}{\partial t} \approx \beta_r v_\theta \\ \beta_r = \dfrac{2\Omega_0 \sin\theta}{r} \end{cases}$$

(planetary)
β-effect

- equatorial mode
- retrograde propagation
- non-convecting

[Rossby 1939,1940, Saio 1982]

thermal Rossby wave

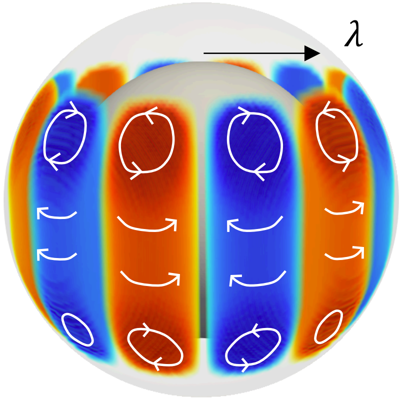

$$\begin{cases} \dfrac{\partial \zeta_z}{\partial t} \approx \beta_c v_\lambda \\ \beta_c = -\dfrac{2\Omega_0 \sin\theta}{H_\rho} \end{cases}$$

compressional
β-effect

- equatorial mode
- prograde propagation
- **convectively-driven**

[e.g., Busse 1970, Miesch et al., 2008]

topographic Rossby wave

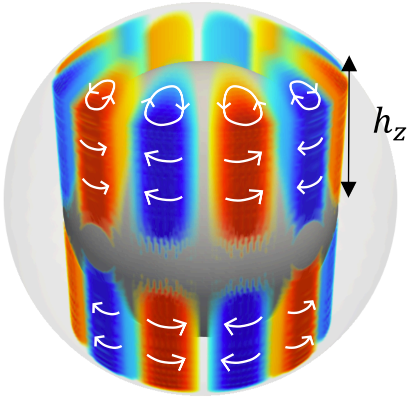

$$\begin{cases} \dfrac{\partial \zeta_z}{\partial t} \approx \beta_t v_\lambda \\ \beta_t = 2\Omega_0 \left(\dfrac{d\ln h_z}{d\lambda}\right) \end{cases}$$

topographic
β-effect

- high-latitude mode
- retrograde propagation
- non-convecting

I. Traditional Rossby waves (r-modes)

- Near the equator, **Rossby waves (r-modes)** have been robustlyobserved at $3 \leq m \leq 15$
- They contribute a significant fraction of the large-scale velocity power at low latitudes
- The observed ridge can be well approximated by the **sectoral mode ($l = m$) r-modes' dispersion relation**
- On the other hand, the observed **eigenfunctions show a significant non-sectoral contribution**

Radial vorticity power spectrum

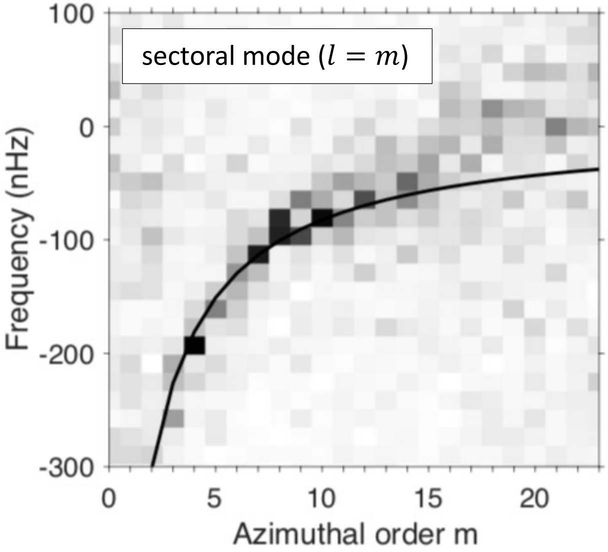

[Löptien et al. 2018]

Latitudinal eigenfunction of radial vorticity

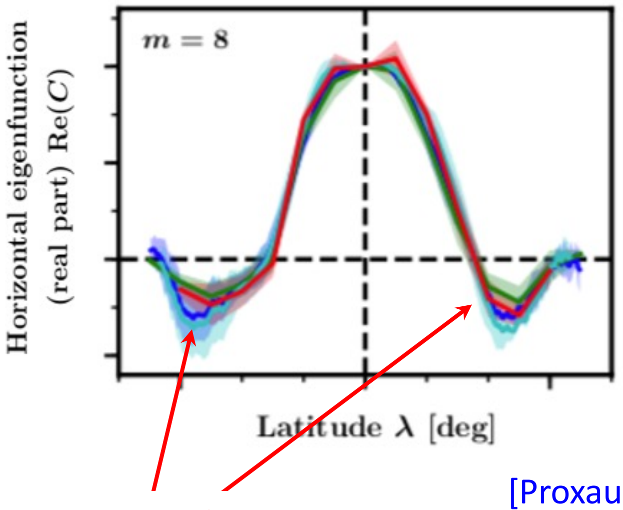

sign changes at mid latitudes

[Proxauf et al. 2020]

II. Thermal Rossby waves (columnar convective modes)

- **Thermal Rossby waves** have been reported many times in numerical simulations as **north-south aligned downflow lanes** across the equator (also called **Banana cells**)
- They are regarded as the **most efficient form of convection** outside the tangential cylinder
- **The origin of solar differential rotation** is often attributed to thermal Rossby waves
- However, **they have NEVER been successfully detected on the Sun**

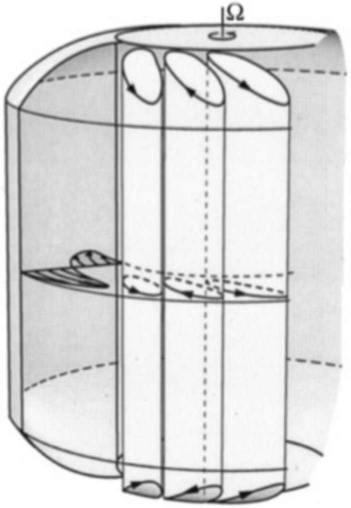

[Busse 2002]

[Caution] topographic β-effect is considered in the geophysical context

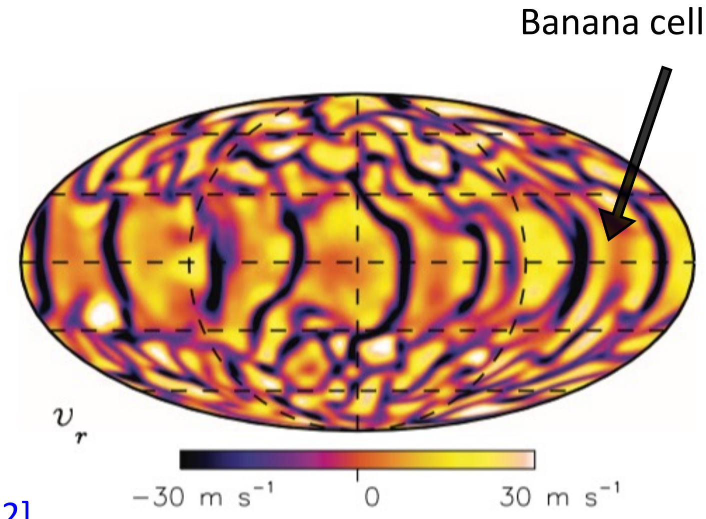

[Miesch et al. 2006]

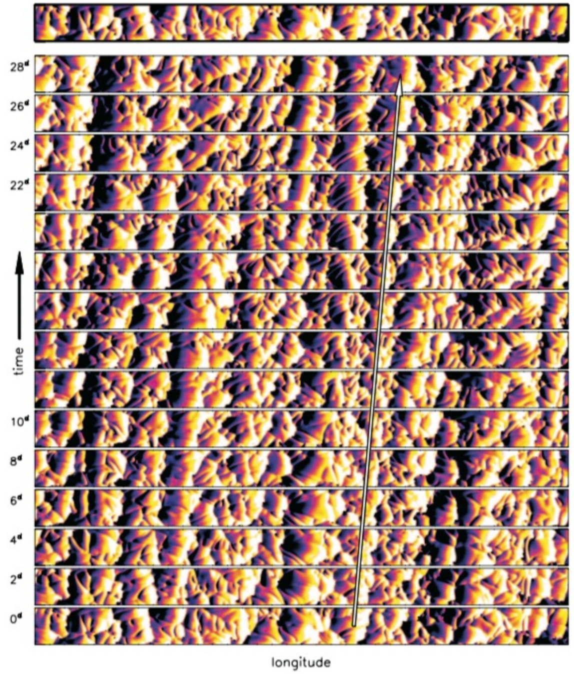

[Miesch et al. 2008]

III. Topographic Rossby waves (high-latitude modes)

- **Topographic Rossby waves** have never been discussed in the solar context in previous literature
- Observations show the **m=1 flow feature at high-latitudes** **that spirals towards the poles**
- Some people argue that this high-latitude flow represents the deep-seated giant cell convection
- We will argue that the **high-latitude observations can be explained in terms of topographic Rossby waves**

  (and baroclinic instability)

Observational snapshot of the non-axisymmetric v_ϕ

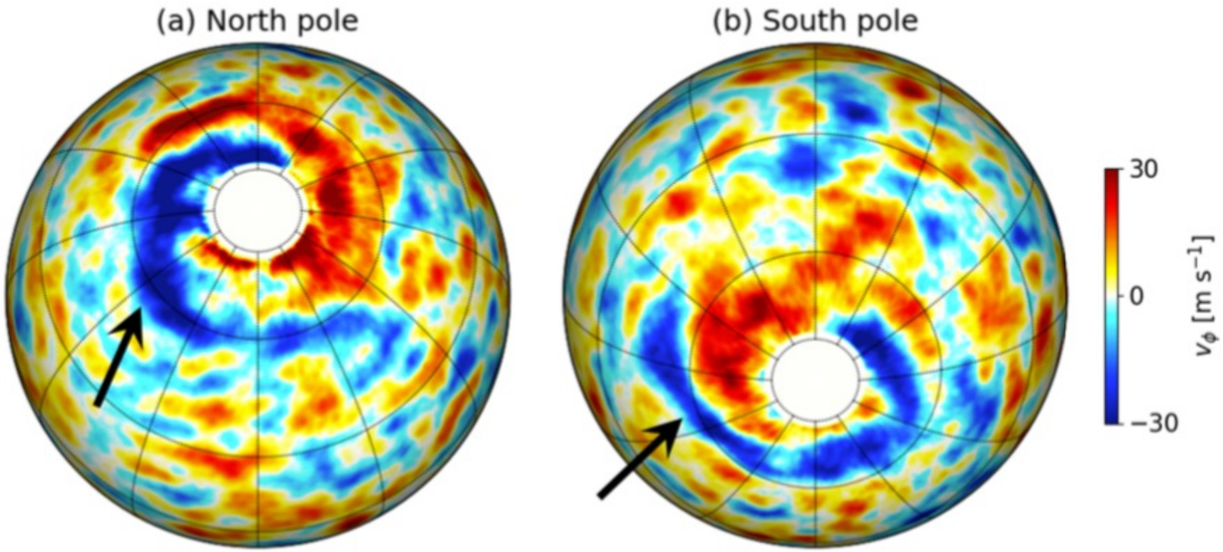

[Data provided by Hathaway & Upton., 2013, 2020]

Outline of this talk

- **Linear analysis of Rossby waves in the Sun**
  - Dispersion relation and eigenfunctions of equatorial modes
  - Discovery of the **"mixed" Rossby modes** between r-modes and thermal Rossby modes

- **Nonlinear rotating convection simulation**
  - Eigen-modes extracted from singular-value-decomposition
  - Interaction between turbulent convection and Rossby waves

---

- **Baroclinic origin of the high-latitude flows in the Sun**
  - Topographic Rossby waves become baroclinically unstable
  - Physical origin of the high-latitude flow spiral
  - Effects of magnetic field and solar dynamo

Outline of this talk

- **Linear analysis of Rossby waves in the Sun**
  - Dispersion relation and eigenfunctions of equatorial modes
  - Discovery of the **"mixed" Rossby modes** between r-modes and thermal Rossby modes
- **Nonlinear rotating convection simulation**
  - Eigen-modes extracted from singular-value-decomposition
  - Interaction between turbulent convection and Rossby waves

---

- **Baroclinic origin of the high-latitude flows in the Sun**
  - Topographic Rossby waves become baroclinically unstable
  - Physical origin of the high-latitude flow spiral
  - Effects of magnetic field and solar dynamo

Linear Model : Eigenmode Solver

- The system equations are linearized and transformed to a pseudo-eigenvalue problem

[Linearized system equations]

$$\frac{\partial \rho_1}{\partial t} = -\nabla \cdot (\rho_0 \boldsymbol{v}) - \Omega_1 \frac{\partial \rho_1}{\partial \phi},$$

$$\frac{\partial \boldsymbol{v}}{\partial t} = -\frac{\nabla p_1}{\rho_0} - \frac{\rho_1}{\rho_0} g \boldsymbol{e}_r - \Omega_1 \frac{\partial \boldsymbol{v}}{\partial \phi} - 2(\Omega_0 + \Omega_1)\boldsymbol{e}_z \times \boldsymbol{v}$$
$$-r \sin\theta \boldsymbol{v} \cdot \nabla \Omega_1 + \frac{1}{\rho_0} \nabla \cdot \boldsymbol{\mathcal{D}},$$

$$\frac{\partial s_1}{\partial t} = -\frac{v_\theta}{r}\frac{\partial s_0}{\partial \theta} - \Omega_1 \frac{\partial s_1}{\partial \phi} + \frac{1}{\rho_0 T_0} \nabla \cdot (\kappa \rho_0 T_0 \nabla s_1).$$

$$\frac{\partial}{\partial t} \Rightarrow -i\omega$$

$$\frac{\partial}{\partial \phi} \Rightarrow im$$

$$\omega \begin{pmatrix} \rho_1 \\ v_r \\ v_\theta \\ v_\phi \\ s_1 \end{pmatrix} = \underbrace{\overbrace{\begin{pmatrix} & & \\ & \widehat{\boldsymbol{M}}(m, \Omega_1) & \\ & & \end{pmatrix}}^{5N_r N_\theta}}_{5N_r N_\theta} \begin{pmatrix} \rho_1 \\ v_r \\ v_\theta \\ v_\phi \\ s_1 \end{pmatrix} \quad N_r N_\theta$$

- Spatial derivatives are evaluated with 4th-order central difference method
- Boundary conditions (closed and stress-free) are incorporated in the differential operator
- The eigenvalue equation is solved numerically and focus on the low-frequency modes ($|\Re[\omega]| < 2\Omega_0$)
- The **solar model S** is used for the background stratification
- We begin our analysis for **inviscid, uniformly-rotating Sun**
- Then, add the turbulent diffusivities, differential rotation, and the background entropy variation

Bekki et al. 2021b (to be submitted)

Linear Results : r-modes with no radial nodes (n=0)

(a) $m = 2$

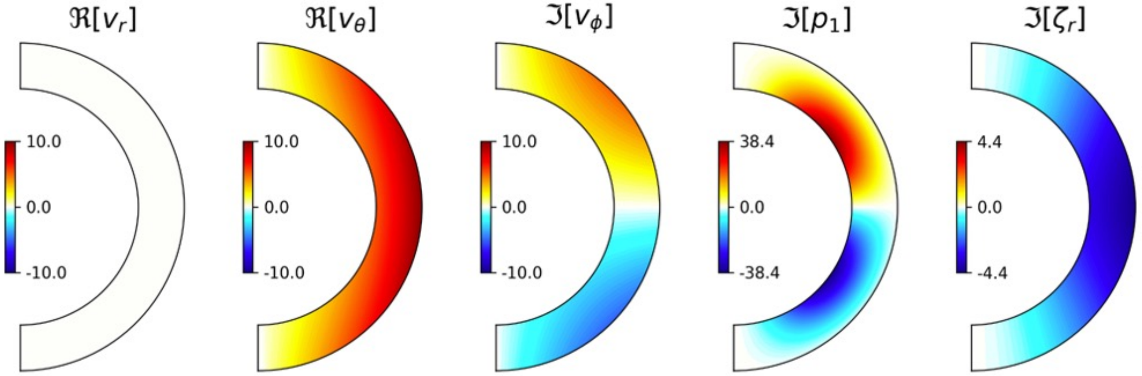

(c)

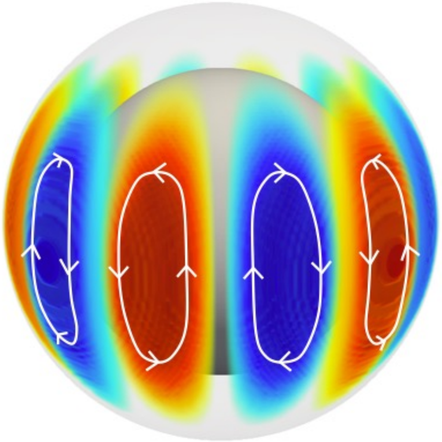

(b) $m = 8$

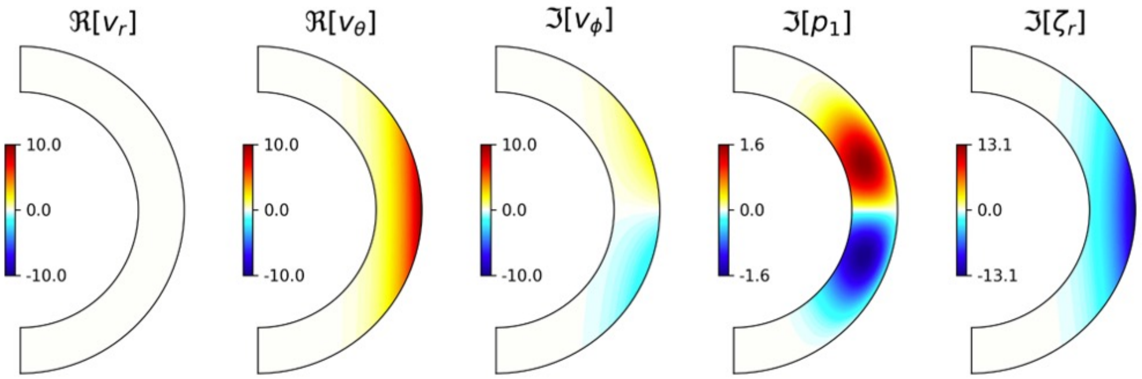

(d)

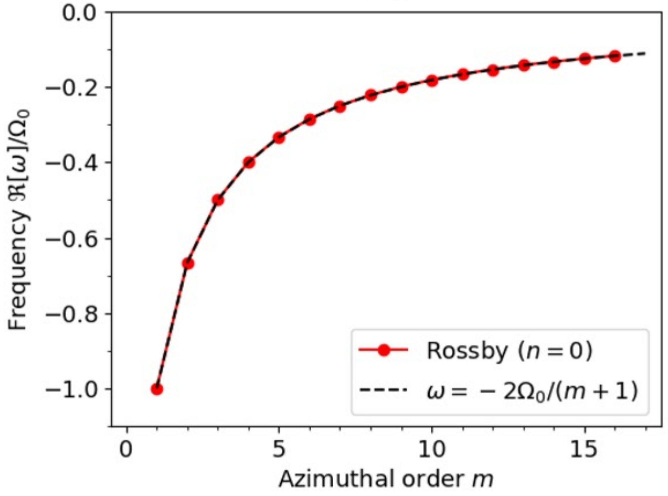

Linear Results : r-modes with no radial nodes (n=0)

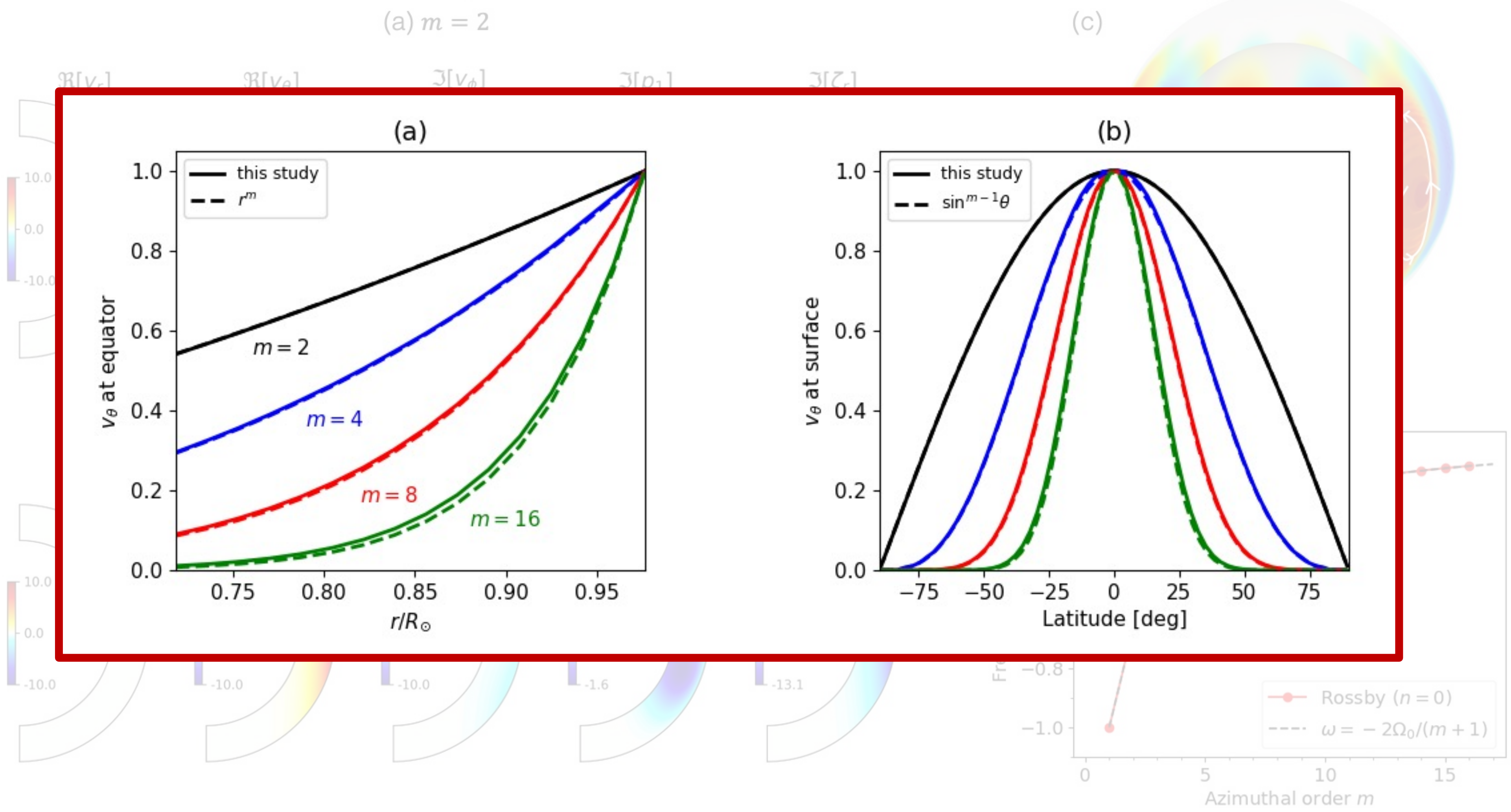

Linear Results : Thermal Rossby waves (ζ_z symm)

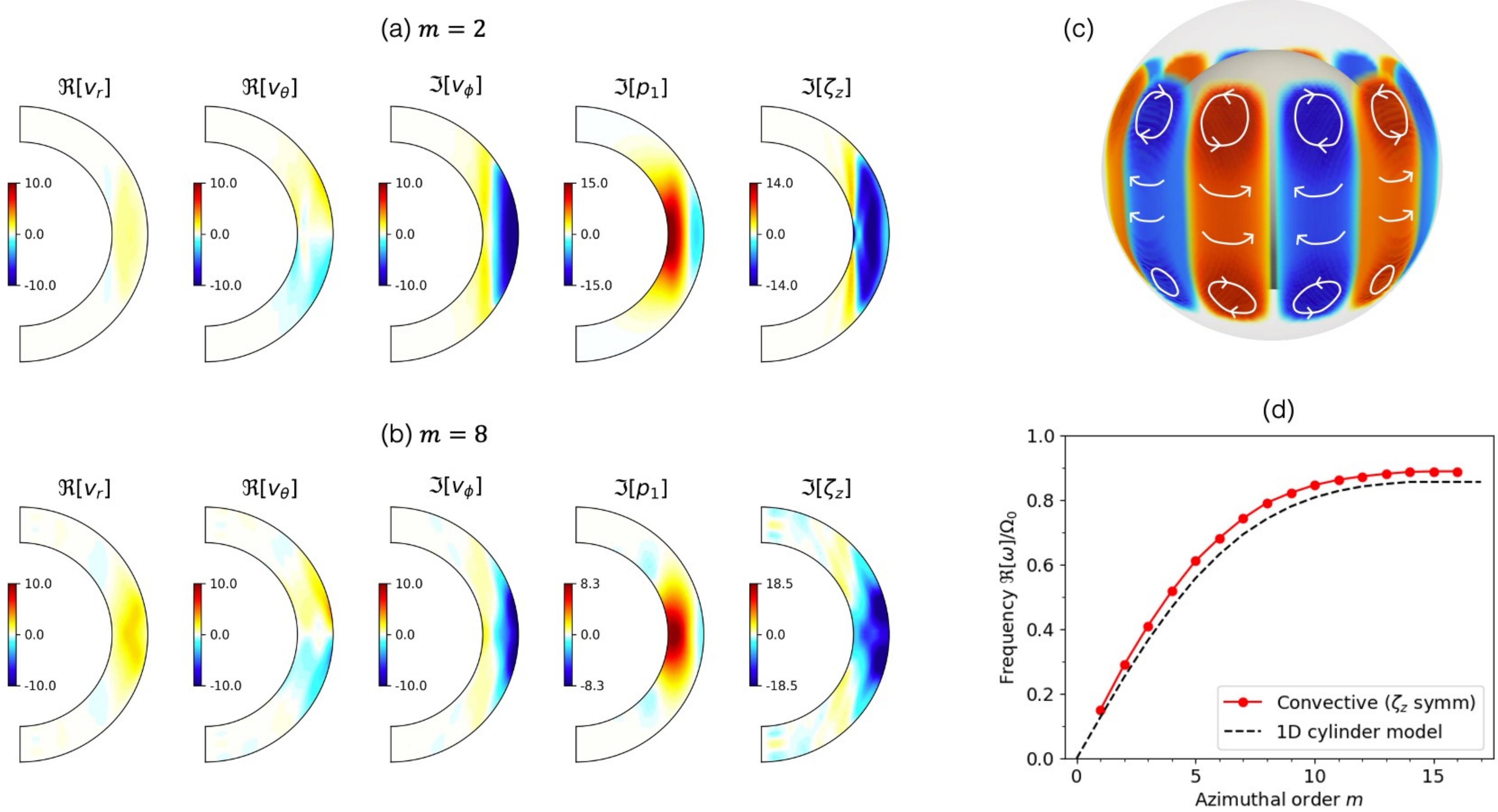

Linear Results : Topographic Rossby waves (ζ_z symm)

(a) $m = 2$

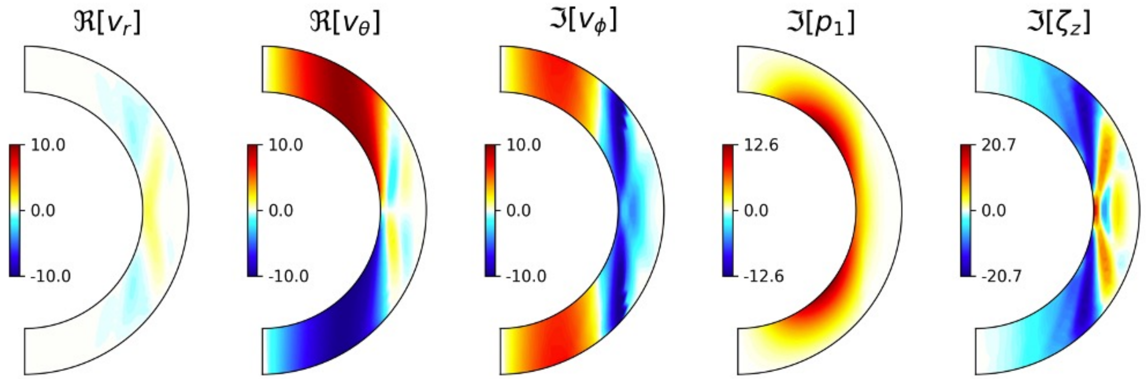

(b) $m = 8$

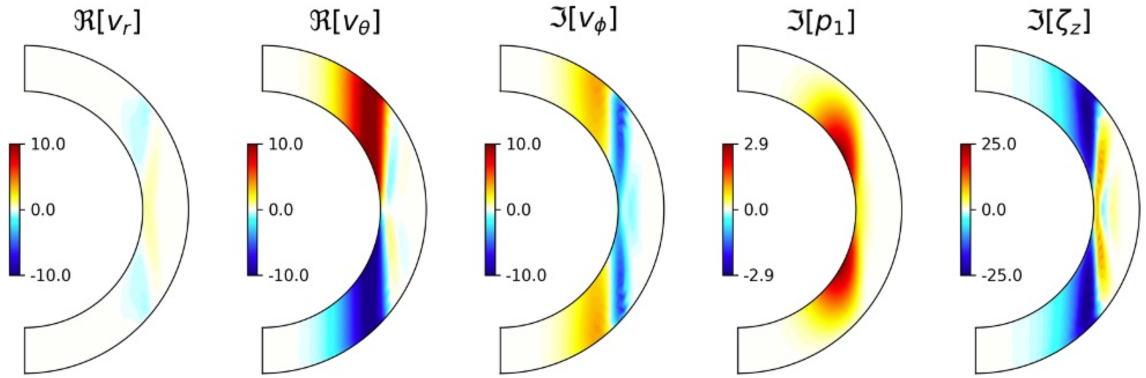

(c)

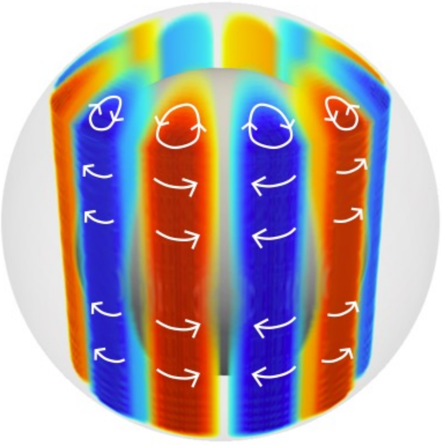

(d)

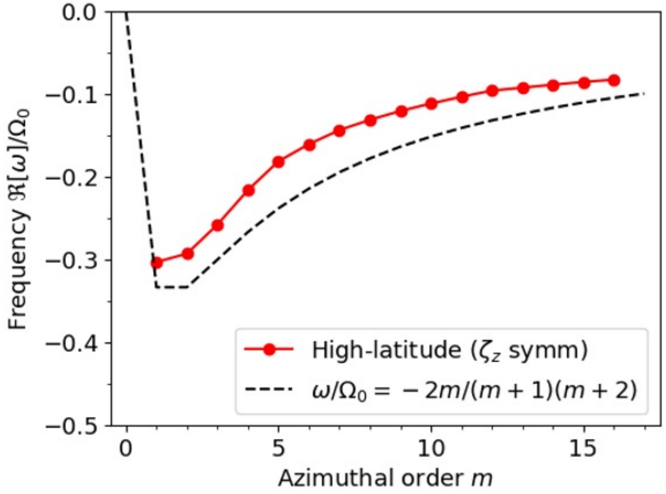

[Glatzmaier & Gilman 1981]

Linear Results : Topographic Rossby waves (ζ_z anti-symm)

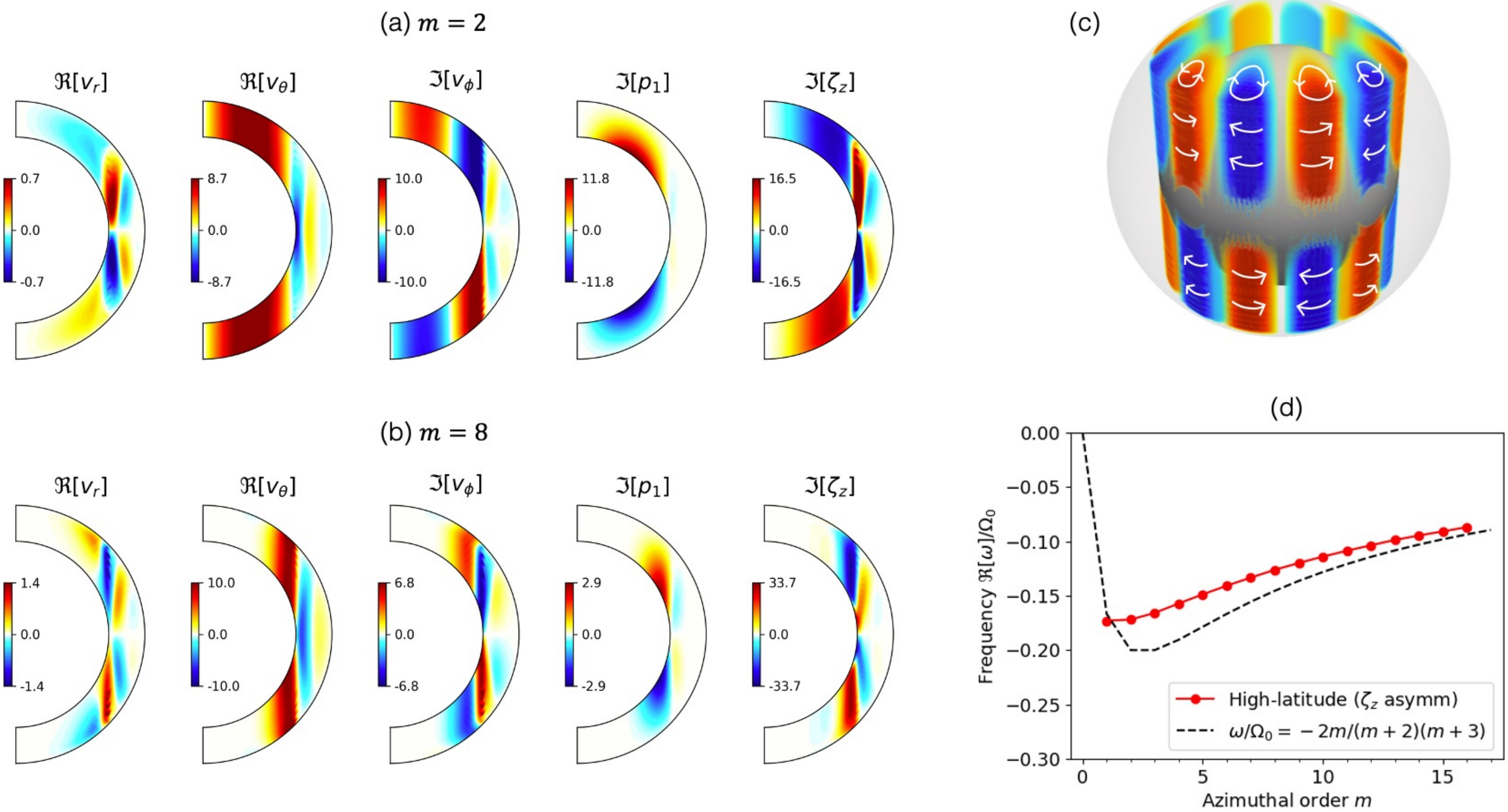

Linear Results : “Mixed” Rossby modes

- We find that the r-modes with **one radial node (n=1)** and the thermal Rossby waves with **north-south anti-symmetric ζ_z** are mixed with one another, forming the **“mixed” Rossby modes**
- This mode coupling can be understood in analogous to “Yanai” waves (mixed Rossby gravity waves)

r-modes
(n=1)

thermal Rossby
(anti-symm)

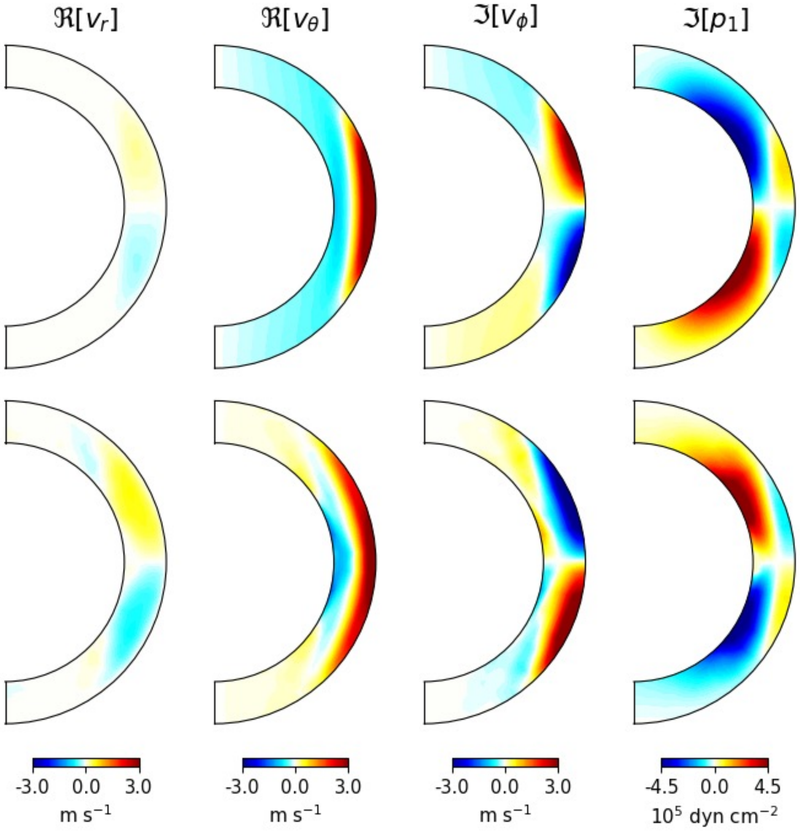

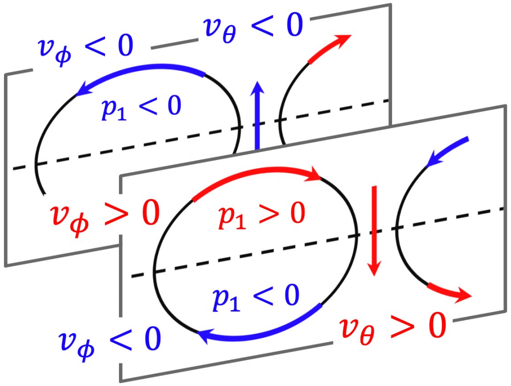

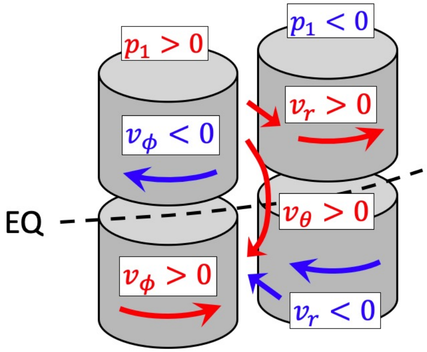

Linear Results : “Mixed” Rossby modes

- We find that the r-modes with **one radial node (n=1)** and the thermal Rossby waves with **north-south anti-symmetric ζ_z** are mixed with one another, forming the **“mixed” Rossby modes**
- This mode coupling can be understood in analogous to “Yanai” waves (mixed Rossby gravity waves)

r-modes
(n=1)

thermal Rossby
(anti-symm)

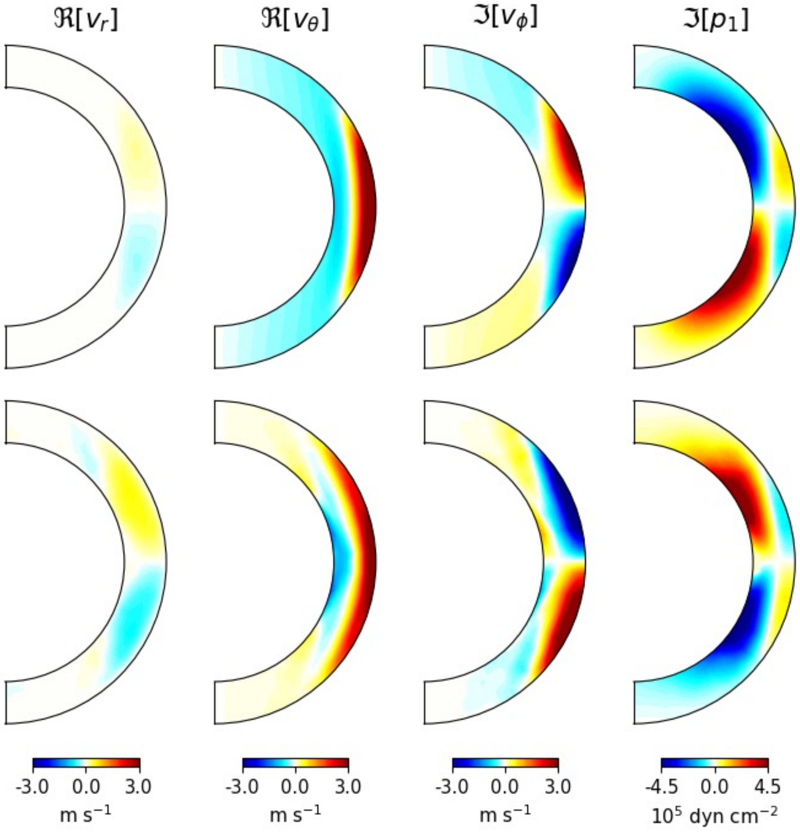

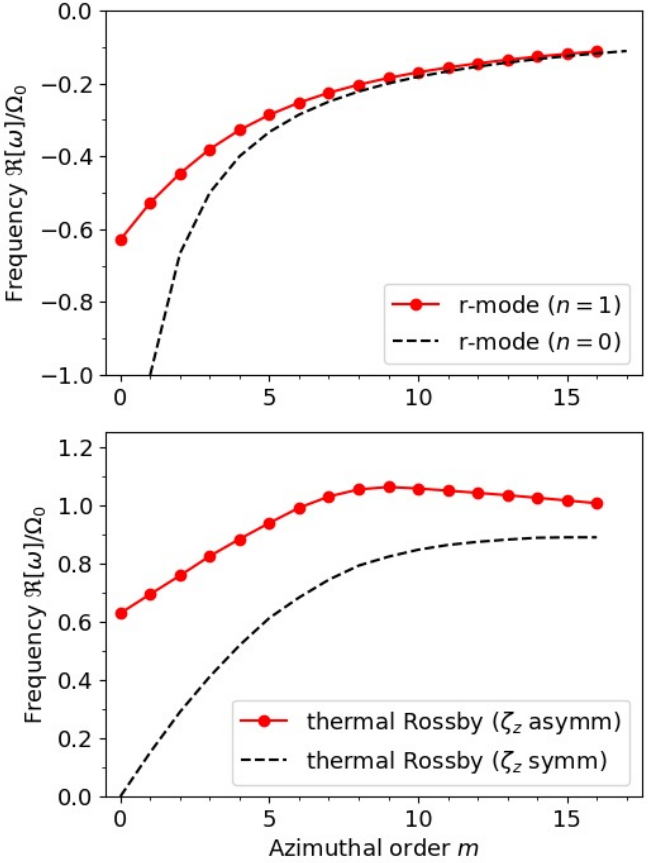

Linear Results : "Mixed" Rossby modes

- We find that the r-modes with **one radial node (n=1)** and the thermal Rossby waves with **north-south anti-symmetric ζ_z** are mixed with one another, forming the **"mixed" Rossby modes**
- This mode coupling can be understood in analogous to "Yanai" waves (mixed Rossby gravity waves)

r-modes
(n=1)

thermal Rossby
(anti-symm)

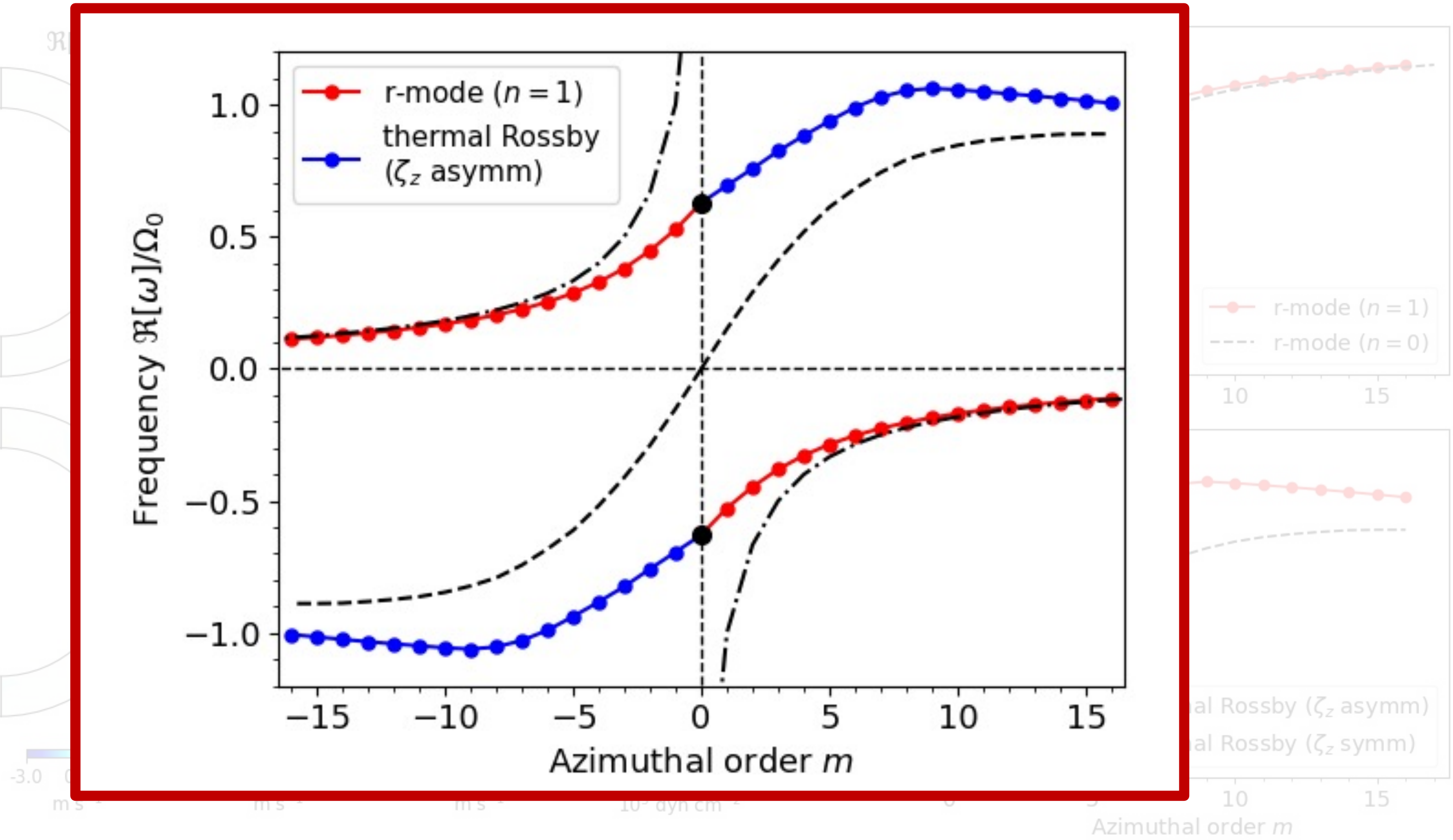

Effect of Turbulent Diffusivities in the Sun on r-modes

- When moderate turbulent diffusion is added, the n=0 r-modes are more and more shifted downwards, leading to a significant deviation from the well-known r^m dependence
- This is likely due to the imbalance of the radial forces and downward diffusive momentum flux
- Consequently, the n=0 modes peak at middle latitudes at the surface in contrast to observations
- On the other hand, the n=1 modes always peak at the surface and at the equator

$n = 0$ eigenfunctions for different turbulent diffusivities

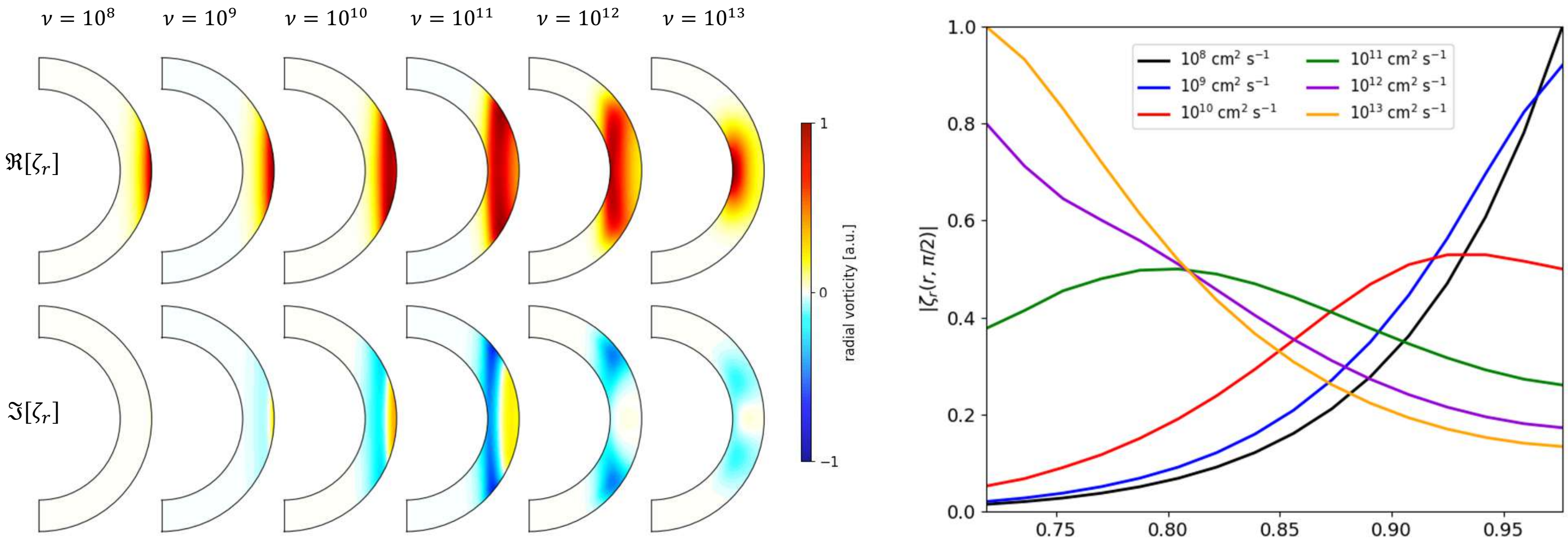

Effect of Solar Differential Rotation on r-modes

- Inclusion of differential rotation introduces **viscous critical layers** where the r-modes' phase speed become equal to the local differential rotation speed
- In the vicinity of the critical layers, strong radial flows are driven and substantial horizontal Reynolds stress are generated, leading to **an equatorward angular momentum transport**

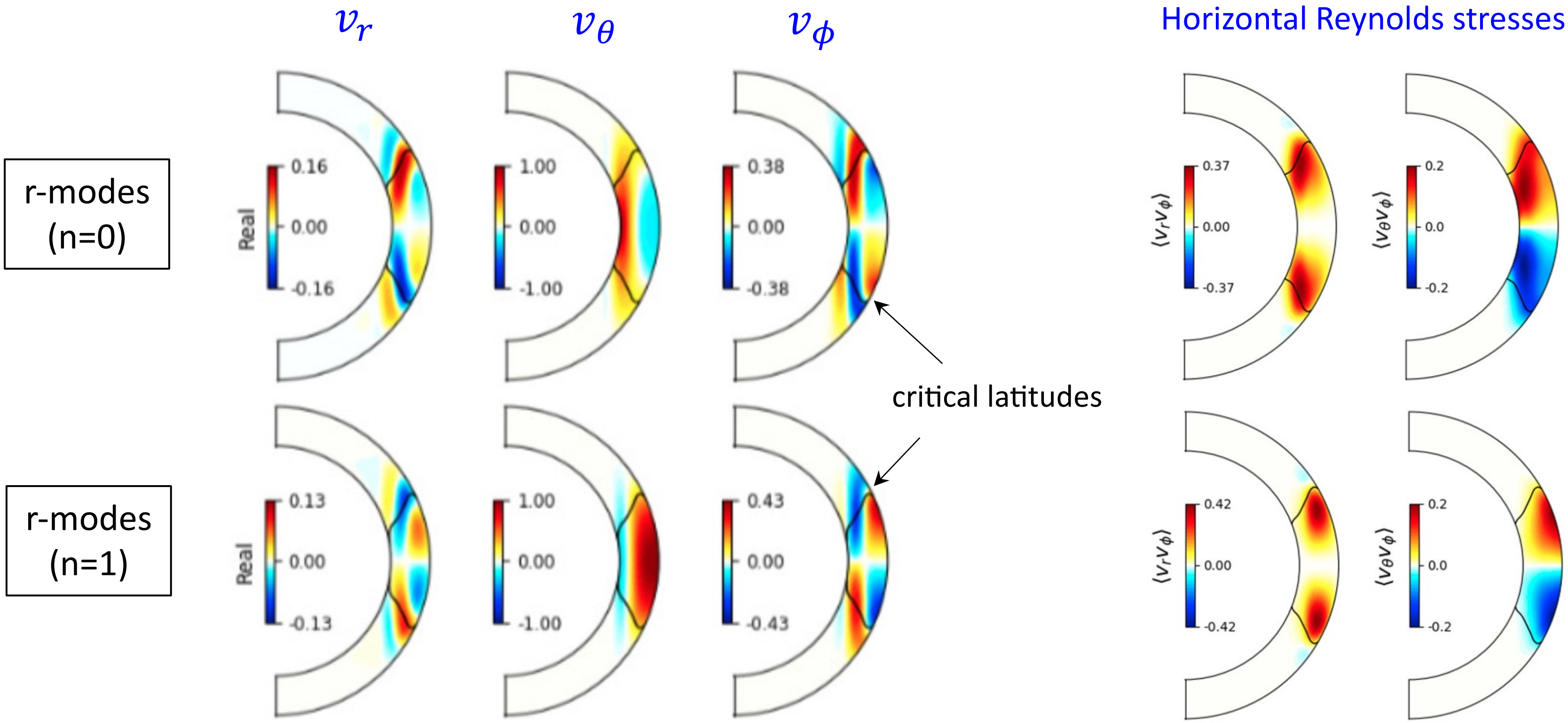

Are the observed Equatorial Rossby modes n=0 or n=1?

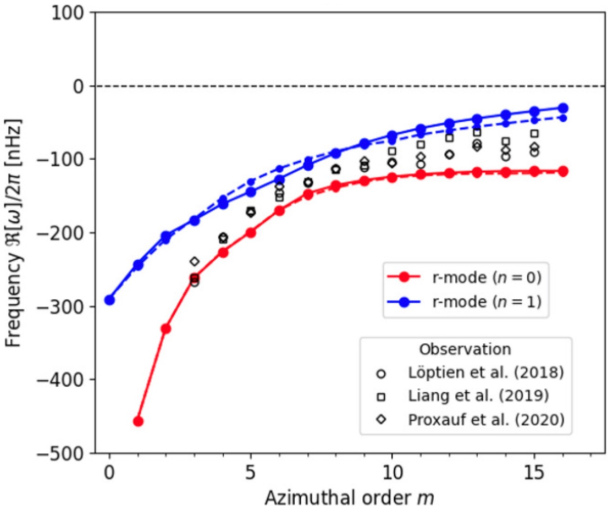

- In terms of the dispersion relation, the observed frequencies lie between those of n=0 and n=1 modes. So, hard to distinguish
- But in terms of the surface eigenfunctions, the **n=1 modes** can give better explanations for the observations
  - prominent peak at the equator
  - sign flip at middle latitudes

surface eigenfunction for (left) n=0 and (right) n=1 r-modes

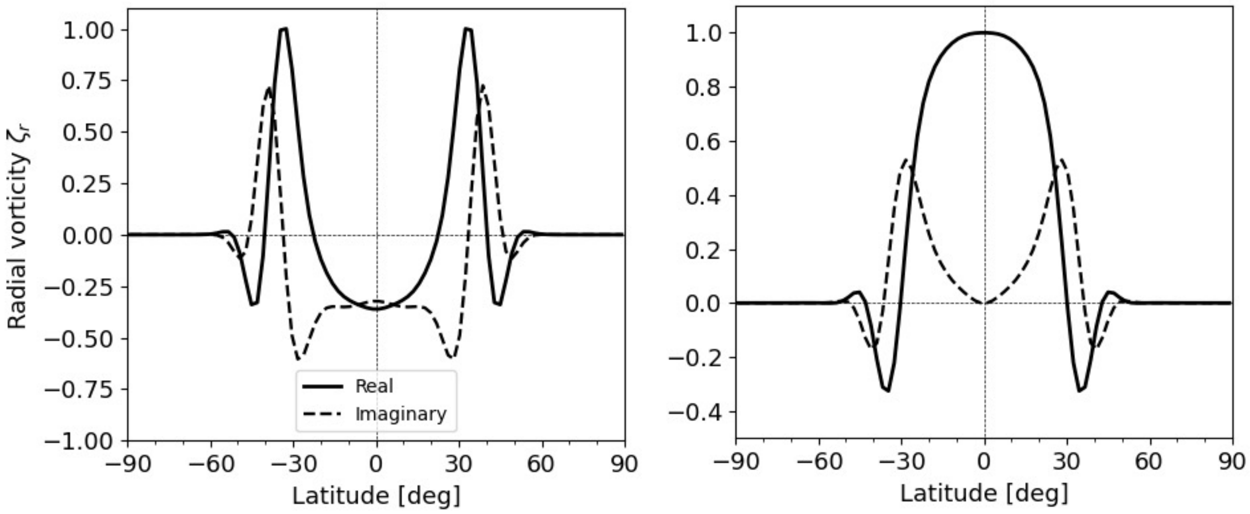

observation

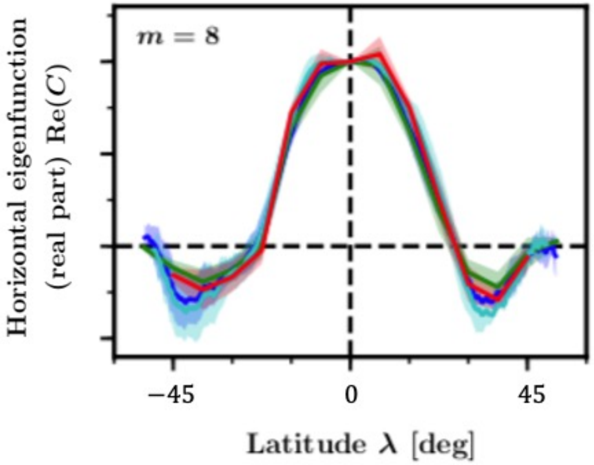

[Proxauf et al. 2020]

Are the observed Equatorial Rossby modes n=0 or n=1?

- In terms of the dispersion relation, the observed frequencies lie between those of n=0 and n=1 modes. So, hard to distinguish
- But in terms of the surface eigenfunctions, the n=1 modes can give better explanations for the observations
    - prominent peak at the equator
    - sign flip at middle latitudes

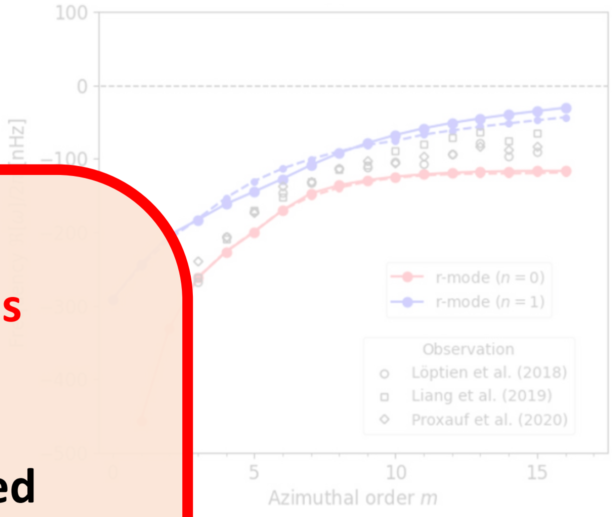

surface eigenfunction for (left) n=0 and (right) n=1 r-modes

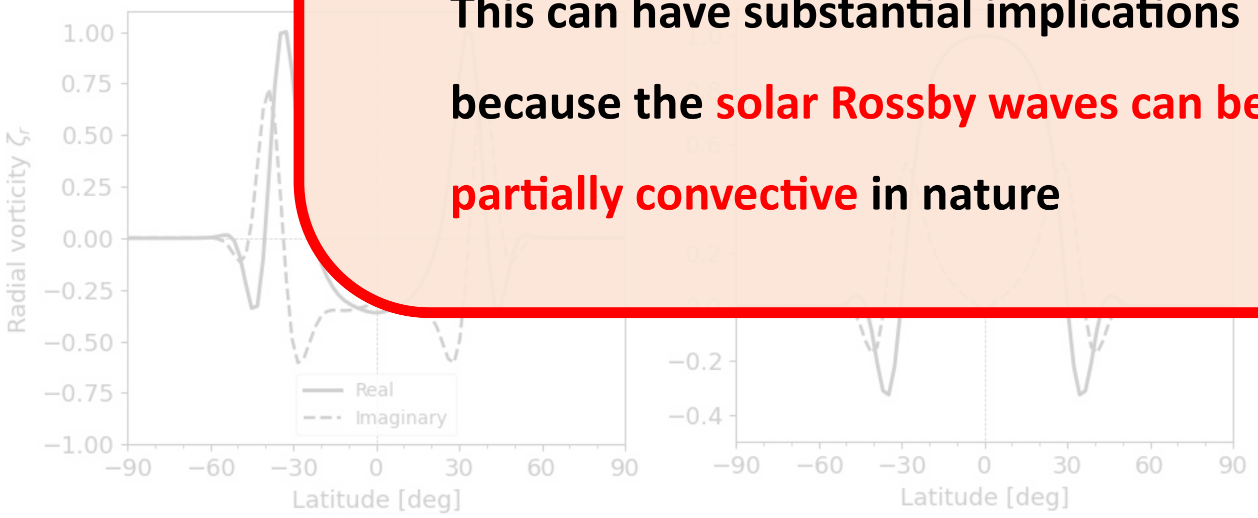

observation

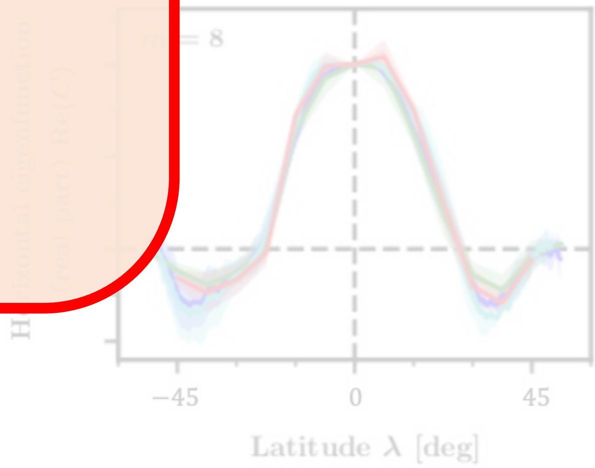

[Proxauf et al. 2020]

We argue that the equatorial Rossby modes observed on the Sun are likely n=1 modes, rather than n=0 modes as normally assumed

This can have substantial implications because the solar Rossby waves can be partially convective in nature

Rossby Waves in a Nonlinear Rotating Convection Simulation

How do these modes (such as newly-discovered “mixed” Rossby modes) behave in the nonlinear regime?

- Full-spherical convection simulation with solar-like stratification from $0.71R_\odot < r < 0.96R_\odot$
- Rotating at the solar rotation rate $\Omega_\odot/2\pi = 431\text{nHz}$ but the luminosity is decreased by a factor of 20 to achieve a solar-like differential rotation (equator acceleration)

[Basic equations]

$$\frac{\partial \rho_1}{\partial t} = -\nabla \cdot [(\rho_0 + \rho_1)\boldsymbol{v}],$$

$$\frac{\partial}{\partial t}(\rho_0 \boldsymbol{v}) = -\rho_0 \boldsymbol{v} \cdot \nabla \boldsymbol{v} - \nabla p_1 + \rho_1 \boldsymbol{g} + 2\rho_0 \boldsymbol{v} \times \boldsymbol{\Omega}_0$$

$$\frac{\partial}{\partial t}(\rho_0 T_0 s_1) = -\rho_0 T_0 \boldsymbol{v} \cdot \nabla s_1 + \nabla \cdot (\rho_0 T_0 \kappa \cdot \nabla s_1) + Q_{\rm rad} + Q_{\rm vis}$$

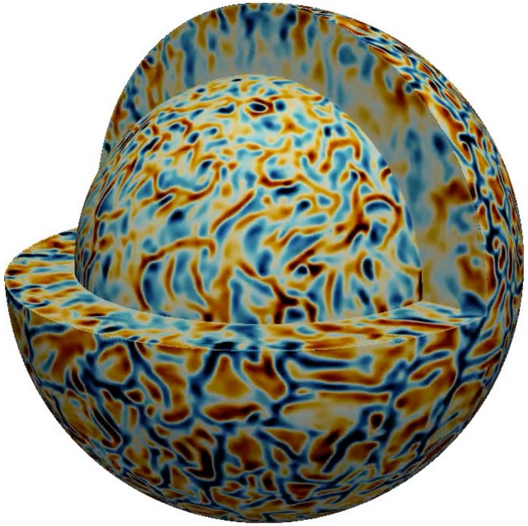

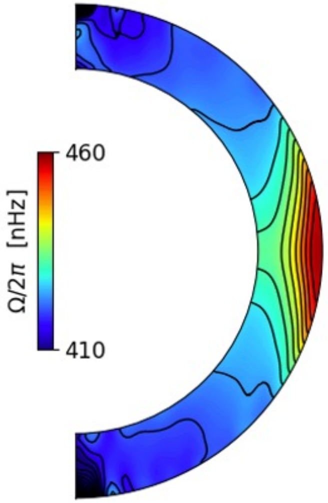

- Total 15 year time series of data with a 5 day cadence is analyzed
- We perform a **singular-value decomposition** on the power spectra to filter out the Rossby modes and to extract the eigenfunctions (both real and imaginary parts)

Bekki et al. 2021a (to be submitted)

Nonlinear Simulation : Thermal Rossby waves

- In our convection simulation, **thermal Rossby waves** are found to be the most dominant modes in the horizontal velocity power spectrum ($\sim 10^3$ times stronger than the r-modes)
- They transport significant amount of **enthalpy** and **angular momentum**

$l = m$ power spectrum of v_ϕ

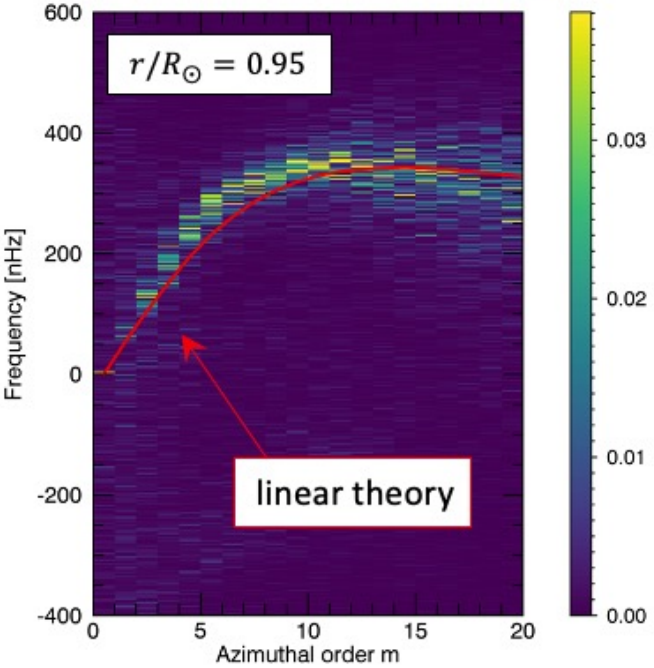

Eigenfunction of $m = 2$

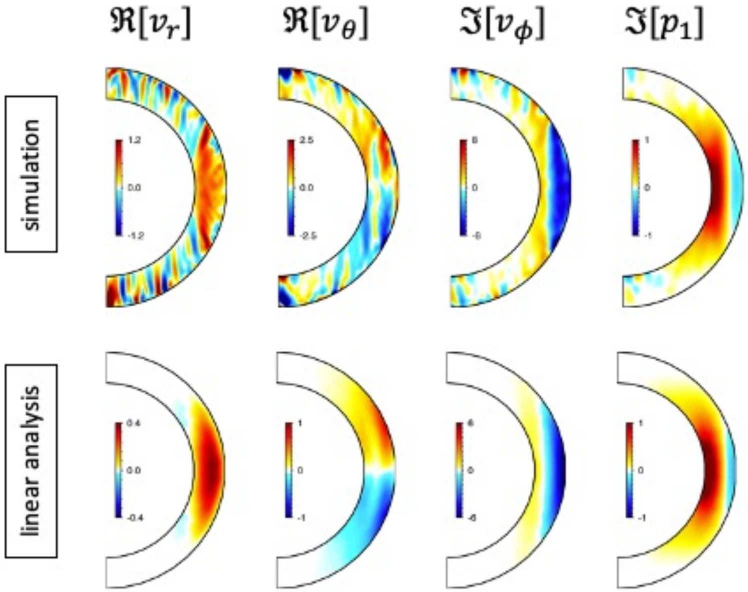

Enthalpy flux

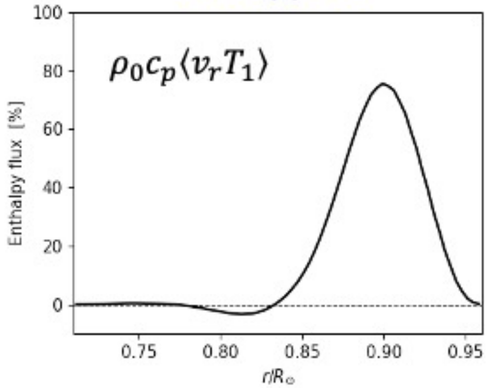

Reynolds stress

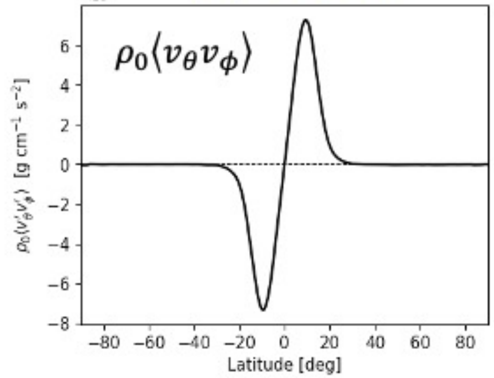

Nonlinear Simulation : r-modes ($n = 0$)

- A well-defined power ridge can be seen in the sectoral mode Rossby wave dispersion relation
- At low-*m*, r-mode exists globally in radius (**radial node *n=0***)
- At higher-*m*, the mode tends to be strongly confined near the base of the convection zone

$l = m$ power spectrum of v_θ

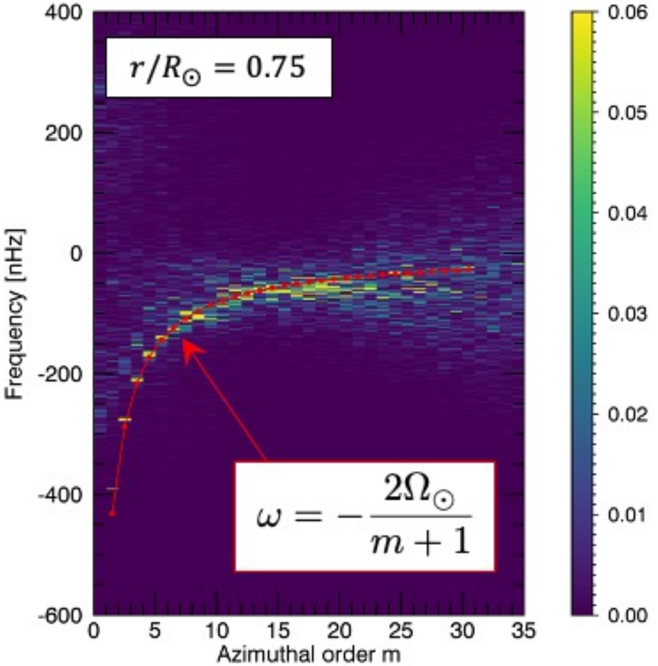

Eigenfunction of $m = 2$

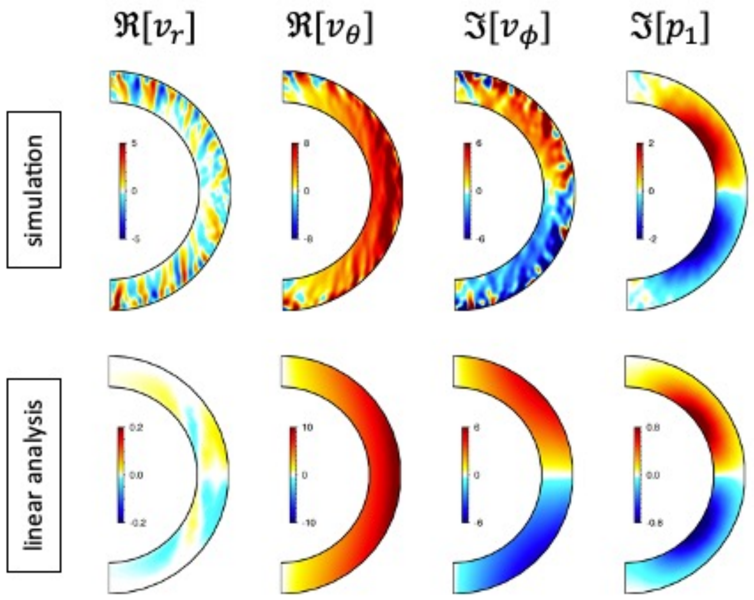

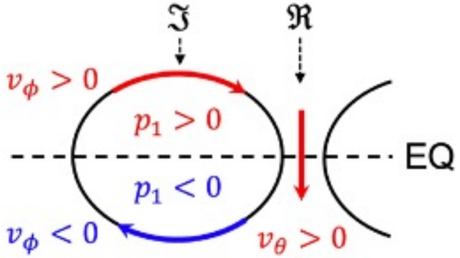

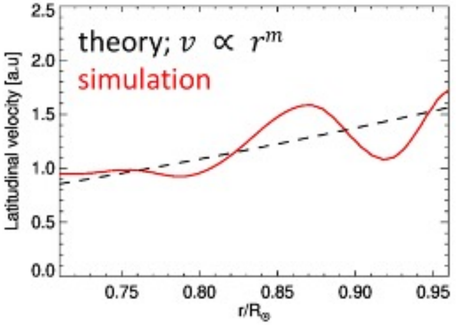

Nonlinear Simulation : r-modes ($n = 0$)

- A well-defined power ridge can be seen in the sectoral mode Rossby wave dispersion relation
- At low-*m*, r-mode exists globally in radius (**radial node *n=0***)
- At higher-*m*, the mode tends to be strongly confined near the base of the convection zone

$l = m$ power spectrum of v_θ at $m = 16$

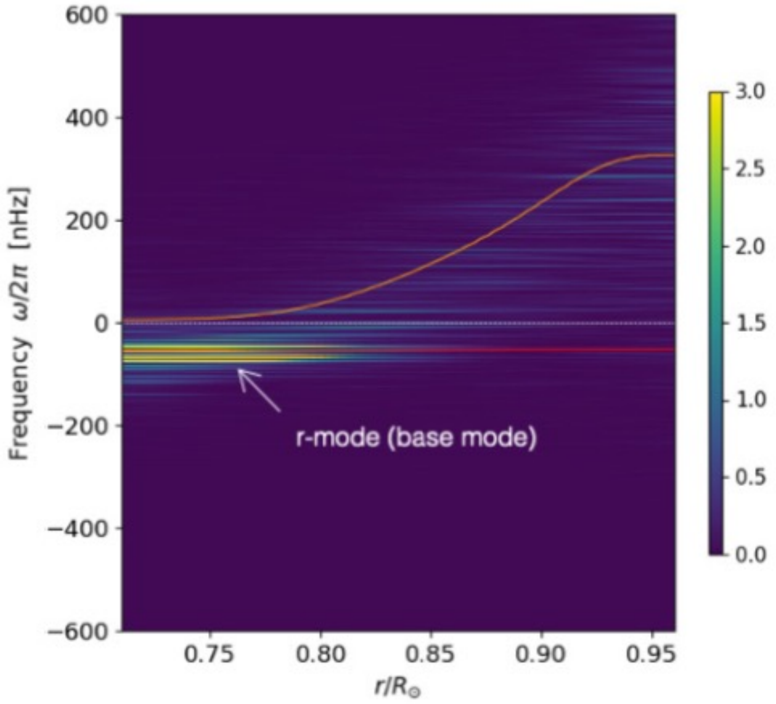

Radial eigenfunctions of
$n = 0$ r-modes at the equator

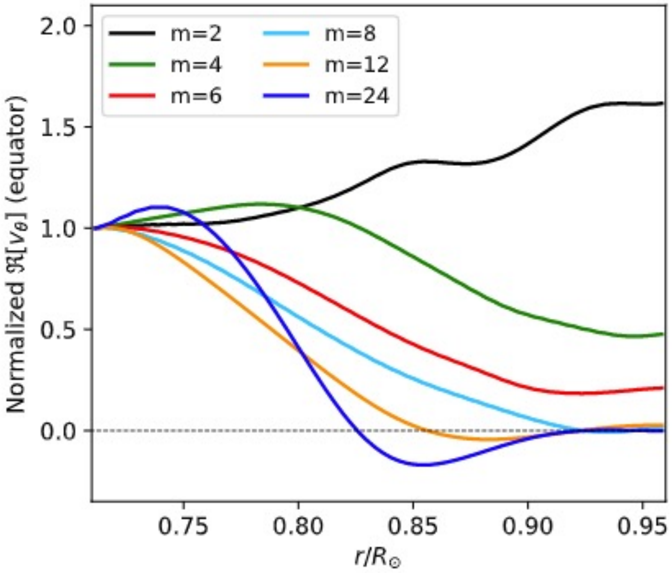

"Mixed" Rossby modes found in the simulation

- We find two distinct oppositely-propagating modes either in the $l = m$ power spectrum of v_θ or $l = m + 1$ spectrum of $\nabla \cdot v_H$ near the surface
- (A) retrograde and (B) prograde mode form a continuous power ridge across $m = 0$

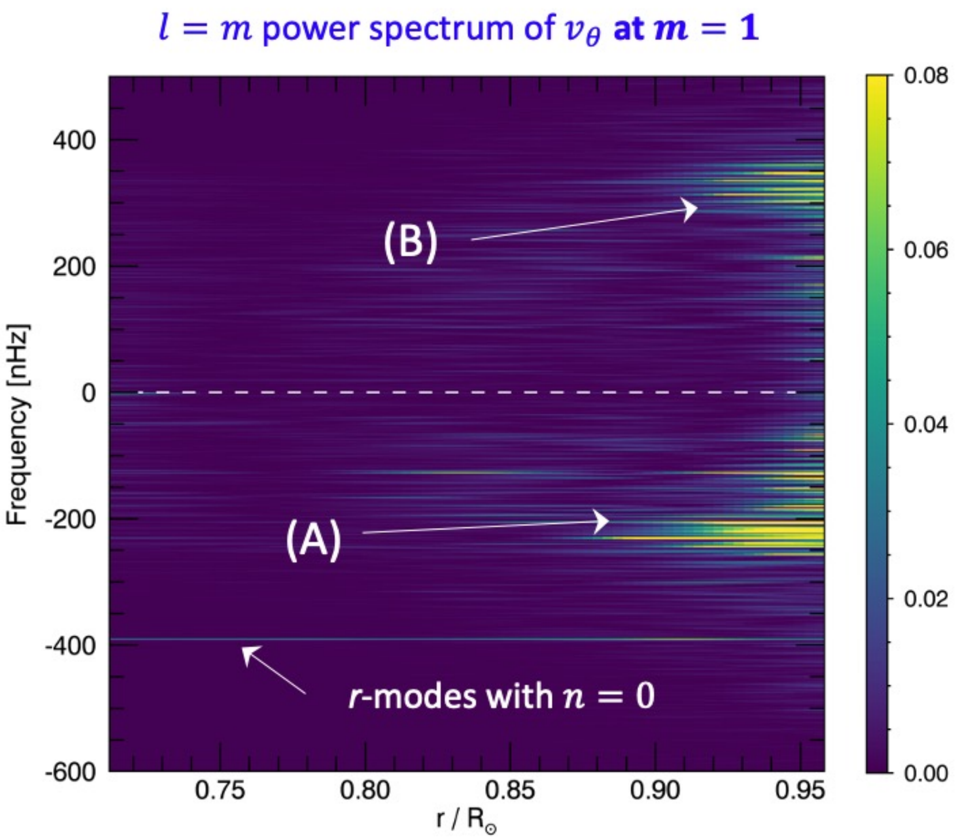

$l = m$ power spectrum of v_θ **at $\boldsymbol{m = 1}$**

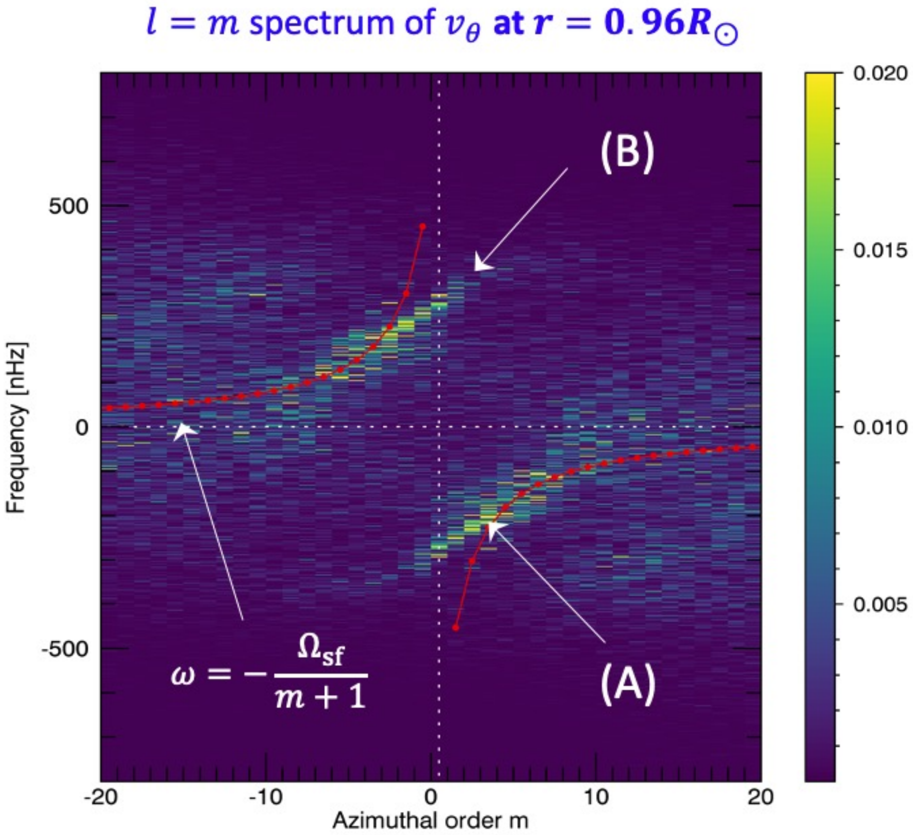

$l = m$ spectrum of v_θ **at $\boldsymbol{r = 0.96 R_\odot}$**

"Mixed" Rossby modes found in the simulation

(A) The retrograde modes are identified as ***r*-modes** with the radial node $n = 1$

(B) The prograde modes are identified as north-south anti-symmetric **thermal Rossby wave**

→ **Mixed Rossby modes between *r*-modes and thermal Rossby waves robustly exist in the rotating convection simulations**

power spectrum at the surface

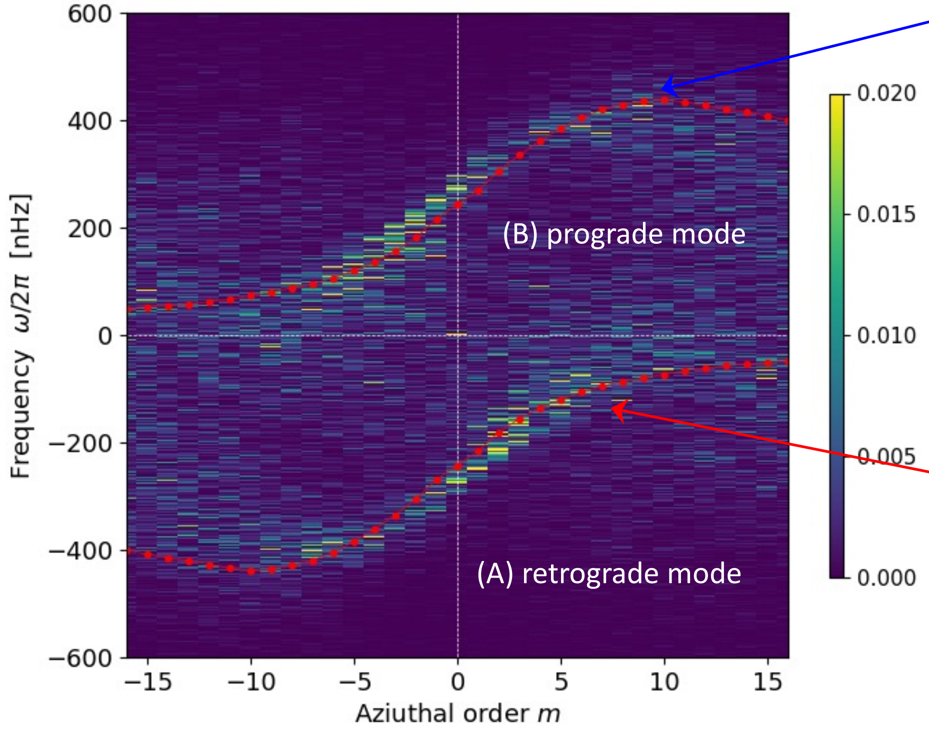

Prograde mode / **anti-symmetric thermal Rossby wave**

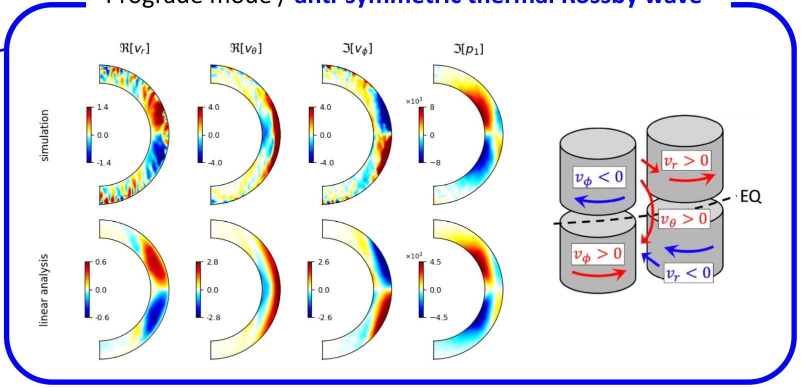

Retrograde mode / **r-mode with one radial node (n=1)**

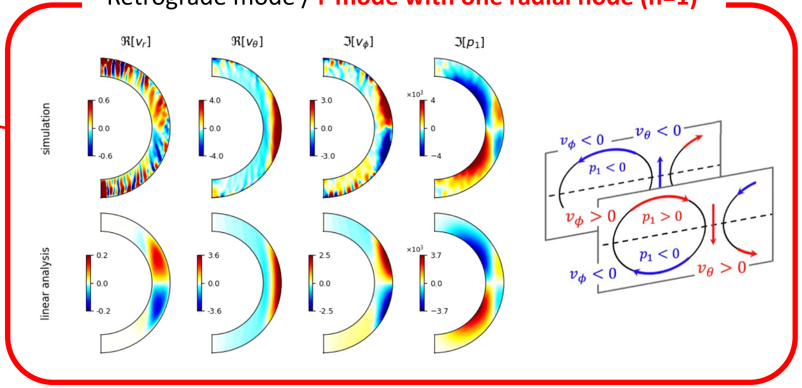

Nonlinear Simulation : Topographic Rossby waves

- At high latitudes, **topographic Rossby waves** are found to exist **inside the tangential cylinder**
- Predominantly exist at **m=1** and propagate in a **retrograde** direction
- However, the observed spiral pattern is not reproduced

← likely due to the lack of strong differential rotation and the baroclinicity (latitudinal entropy variation) in the simulation (to be discussed later)

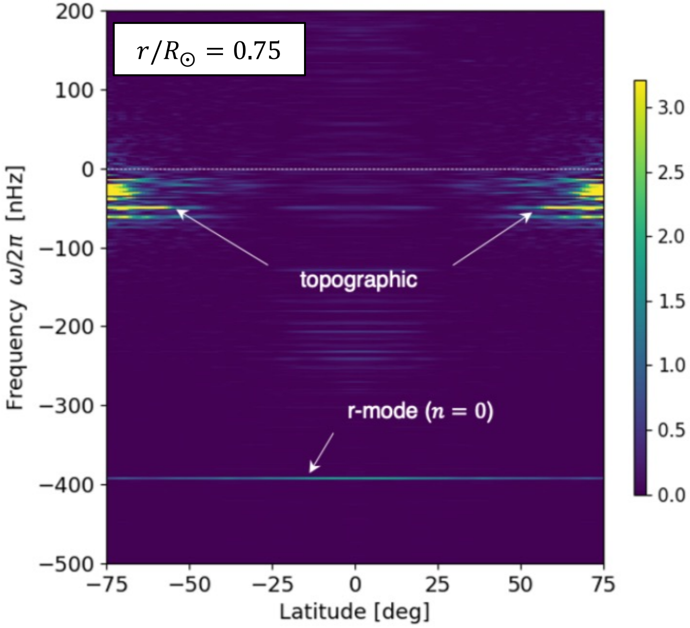

power spectrum of v_θ at $m = 1$

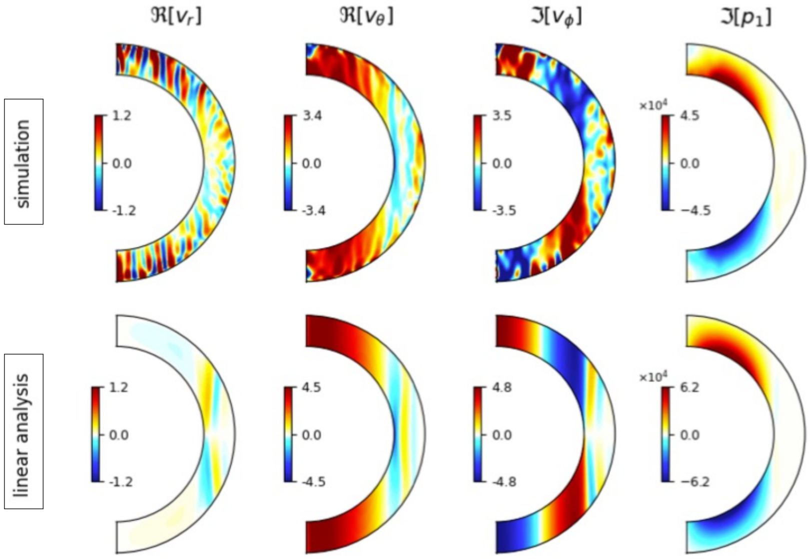

Eigenfunction of $m = 1$

Outline of this talk

- **Linear analysis of Rossby waves in the Sun**
  - Dispersion relation and eigenfunctions of equatorial modes
  - Discovery of the **”mixed” Rossby modes** between r-modes and thermal Rossby modes
- **Nonlinear rotating convection simulation**
  - Eigen-modes extracted from singular-value-decomposition
  - Interaction between turbulent convection and Rossby waves

---

- **Baroclinic origin of the high-latitude flows in the Sun**
  - Topographic Rossby waves become baroclinically unstable
  - Physical origin of the high-latitude flow spiral
  - Effects of magnetic field and solar dynamo

What is baroclinic instability?

- **Baroclinic instability** is a hydrodynamic instability in a **stratified**, **rotating** fluid
- Accompanied by **horizontal temperature gradient** (instability of the **thermal wind**)
- Ubiquitous in Earth's atmosphere, and controls the weather at middle-high latitudes [Vallis 2006]
- Leads to a **formation of large-scale vortices**

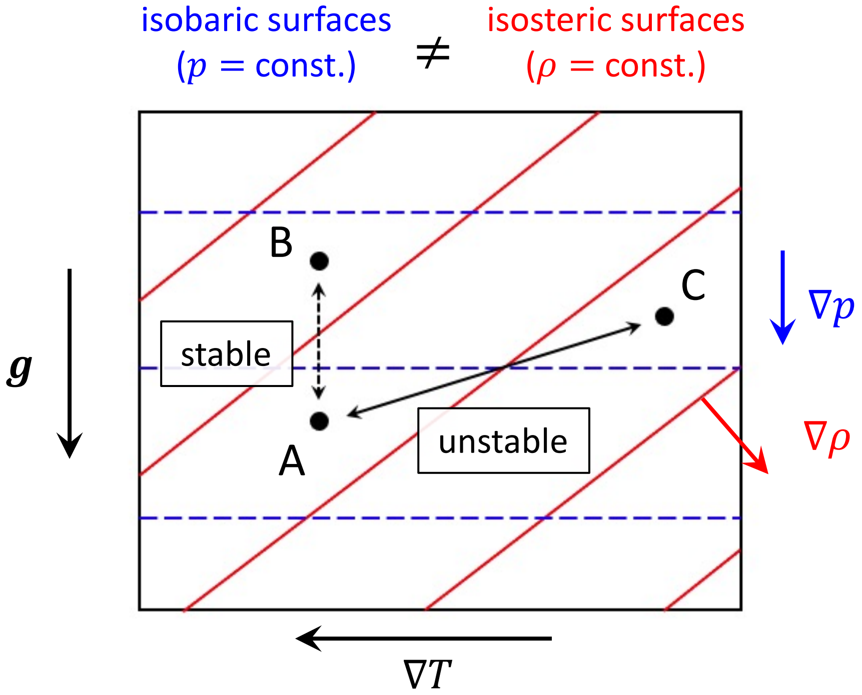

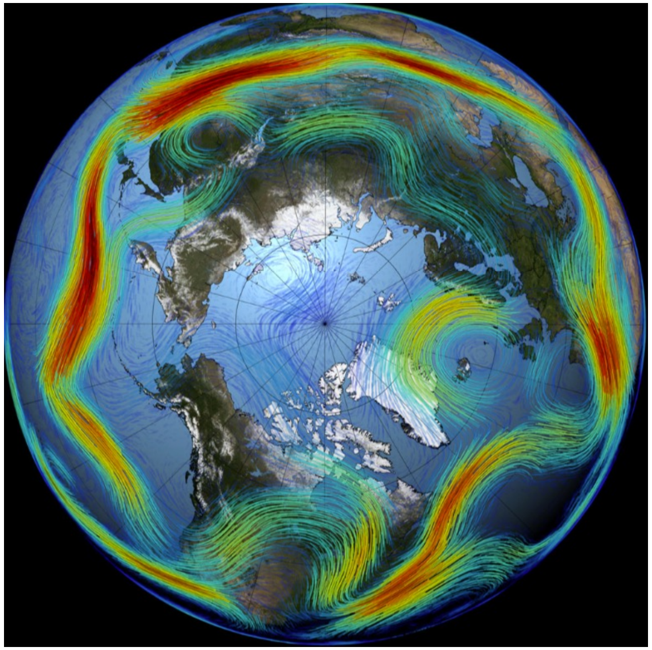

©NASA Scienific visualization studio

Thermal wind balance in the Sun

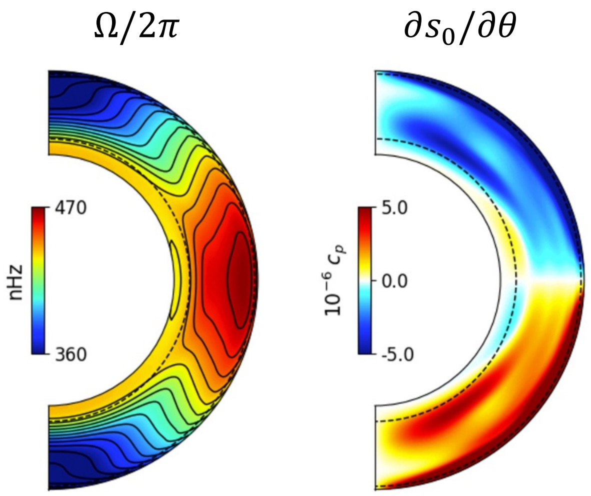

[data from Larson & Schou 2018]

- Differential rotation in the Sun is known to be *baroclinic* (does not follow the Taylor-Proudman's constraint)
- Balanced by **latitudinal entropy (temperature) gradient**

$$\frac{g}{c_p}\frac{\partial s_0}{\partial\theta} = r^2 \sin\theta \frac{\partial\Omega^2}{\partial z}$$

- The required temperature difference between pole-equator is $\lesssim 10$ K [Rempel 2005, Miesch et al. 2006]

- Historically, it has long been believed that **baroclinic instability is** strongly **suppressed** when the stratification is **convectively-unstable** [Knobloch & Spruit 1982,1984]
- However, recent numerical studies indicate that **baroclinic instability can occur even in the presence of convection** [Callies & Farrari 2018]

Linear analysis : Baroclinically-unstable modes

- Without latitudinal entropy gradient $\partial s_0/\partial\theta$, **$m = 1$ topographic Rossby mode** is stable and does not show a spiralling pattern
- **With Increasing $\partial s_0/\partial\theta$, the mode becomes unstable** (growing) even when the background is convectively stable
- The baroclinically-unstable mode show a **spiralling pattern** around the poles similar to the observations
- The **dispersion relation** agrees well with the observations

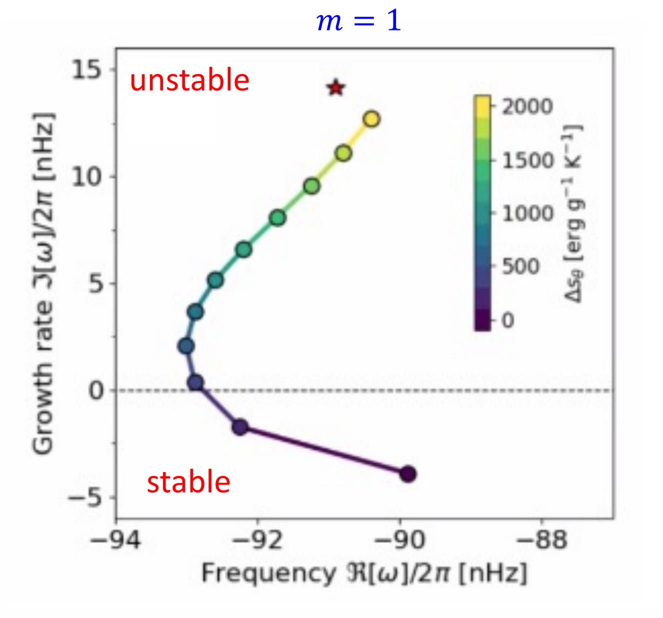

without $\partial s_0/\partial\theta$ (non-baroclinic)

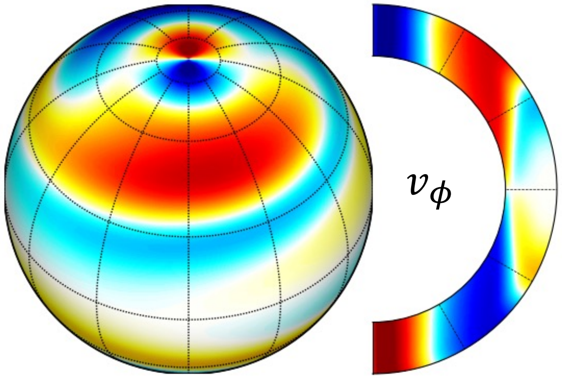

with $\partial s_0/\partial\theta$ (baroclinic)

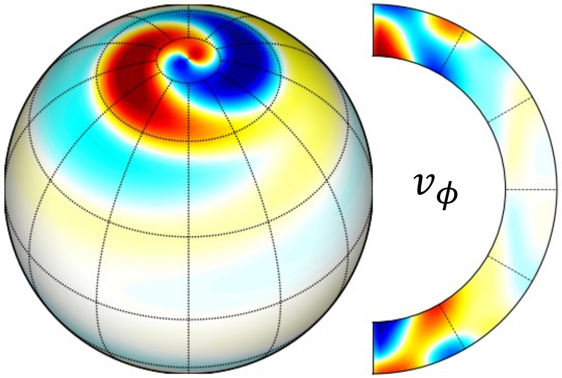

Linear model at $m = 1$

observation

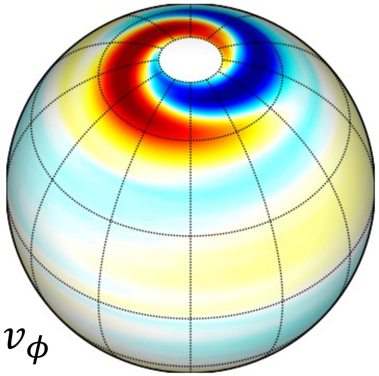

[Gizon et al. 2021]

Linear analysis : Baroclinically-unstable modes

- Without latitudinal entropy gradient $\partial s_0/\partial\theta$, **$m = 1$ topographic Rossby mode** is stable and does not show a spiralling pattern
- **With Increasing $\partial s_0/\partial\theta$, the mode becomes unstable** (growing) even when the background is convectively stable
- The baroclinically-unstable mode show a **spiralling pattern** around the poles similar to the observations
- The **dispersion relation** agrees well with the observations

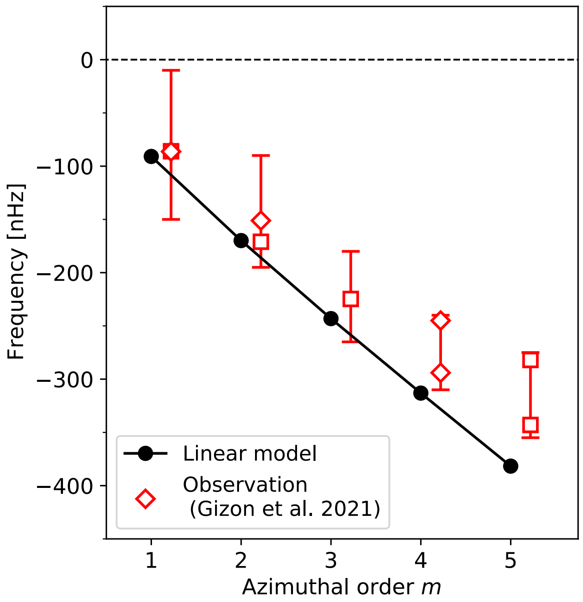

$m = 1$

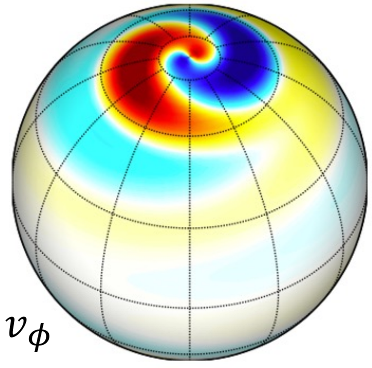

$(-90.1\ \mathrm{nHz}, 14.1\ \mathrm{nHz})$

$m = 2$

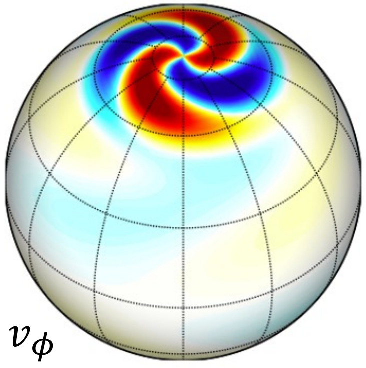

$(-169.9\ \mathrm{nHz}, 23.3\ \mathrm{nHz})$

$m = 3$

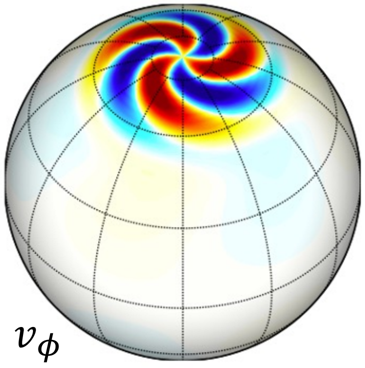

$(-243.1\ \mathrm{nHz}, 24.8\ \mathrm{nHz})$

$m = 4$

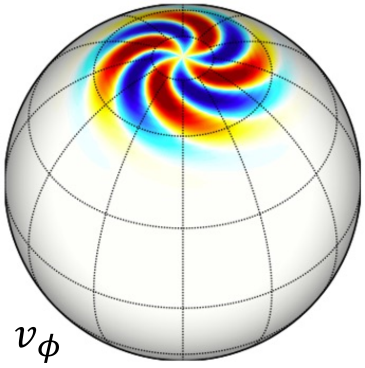

$(-313.1\ \mathrm{nHz}, 29.2\ \mathrm{nHz})$

$m = 5$

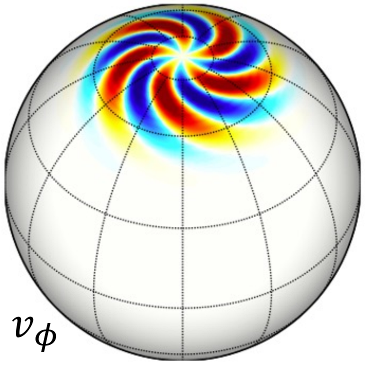

$(-381.7\ \mathrm{nHz}, 33.2\ \mathrm{nHz})$

Nonlinear Model : Full-spherical HD Mean-field Simulations

mass:
$$\frac{\partial \rho_1}{\partial t} = -\frac{1}{\xi^2}\nabla\cdot(\rho_0 \boldsymbol{v}),$$

motion:
$$\frac{\partial \boldsymbol{v}}{\partial t} = -\boldsymbol{v}\cdot\nabla\boldsymbol{v} - \frac{\nabla p_1}{\rho_0} - \frac{\rho_1}{\rho_0} g\boldsymbol{e}_r + 2\boldsymbol{v}\times\Omega_0\boldsymbol{e}_z + \frac{1}{\rho_0}\nabla\cdot\mathcal{R},$$

entropy:
$$\frac{\partial s_1}{\partial t} = \boldsymbol{v}\cdot\nabla s_1 + c_p\delta\frac{v_r}{H_p} + \frac{1}{\rho_0 T_0}\nabla\cdot(\rho_0 T_0 \kappa \nabla s_1) + \frac{1}{\rho_0 T_0}(\mathcal{R}\cdot\nabla)\cdot\boldsymbol{v},$$

- Small-scale convection is **NOT** solved (mean-field)
- **Λ-effect** is parameterized [Kitchatinov & Rudiger 1995]

$$\Pi_{ik} = \rho_0\left[\nu_{\rm vis}\left(S_{ik} - \frac{2}{3}\delta_{ik}\nabla\cdot\boldsymbol{v}\right) + \nu_{\rm lam}\Lambda_{ik}\Omega_0\right]$$

- Weakly subadiabatic layer is included near the base CZ to achieve the thermal wind balance [Rempel 2005]
- We vary the subadiabaticity in the lower CZ ($\boldsymbol{\delta_0}$) that controls the baroclinicity of the system

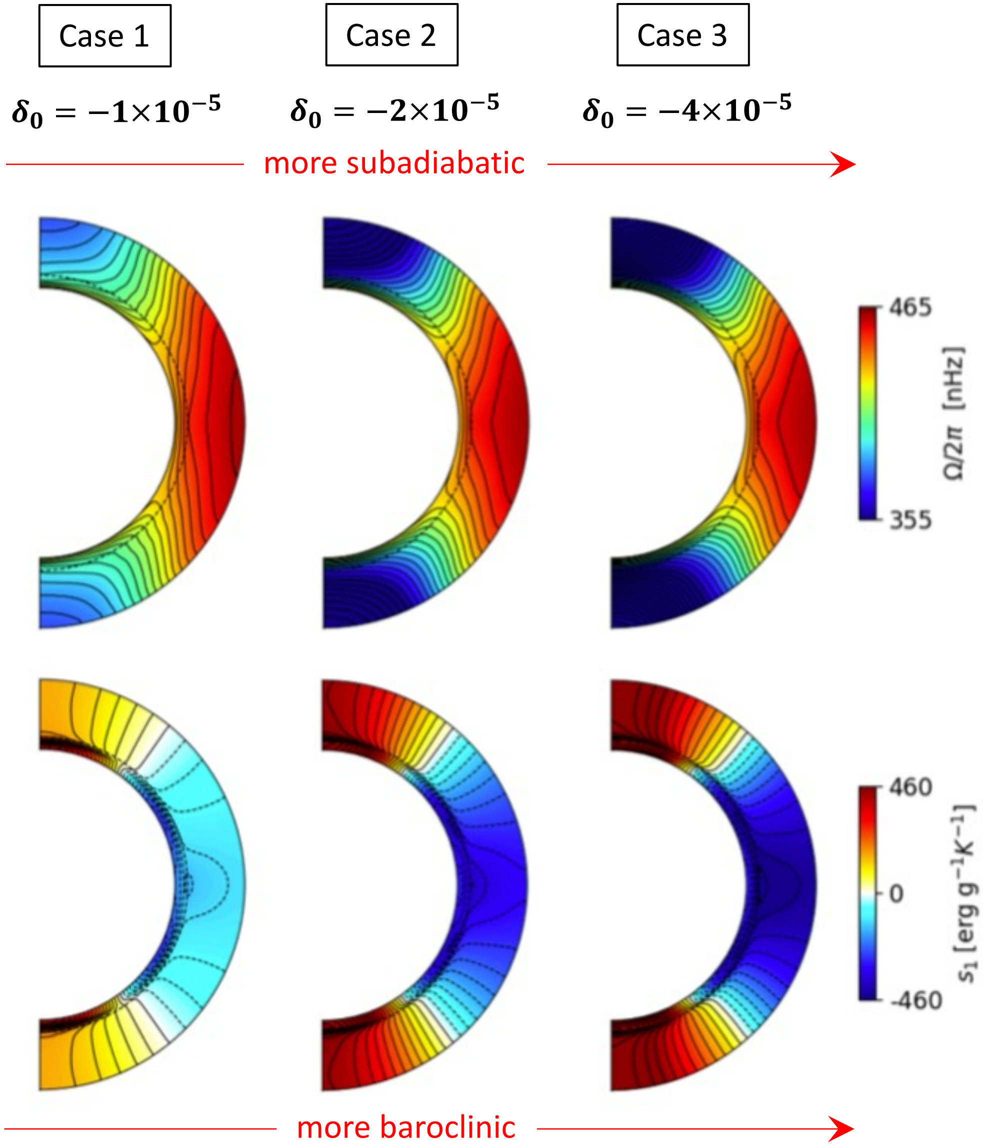

Case 1 $\boldsymbol{\delta_0 = -1\times10^{-5}}$

Case 2 $\boldsymbol{\delta_0 = -2\times10^{-5}}$

Case 3 $\boldsymbol{\delta_0 = -4\times10^{-5}}$

more subadiabatic

more baroclinic

Nonlinear Results : Temporal evolution

Case 1

$\boldsymbol{\delta_0 = -1\times10^{-5}}$

Case 2

$\boldsymbol{\delta_0 = -2\times10^{-5}}$

Case 3

$\boldsymbol{\delta_0 = -4\times10^{-5}}$

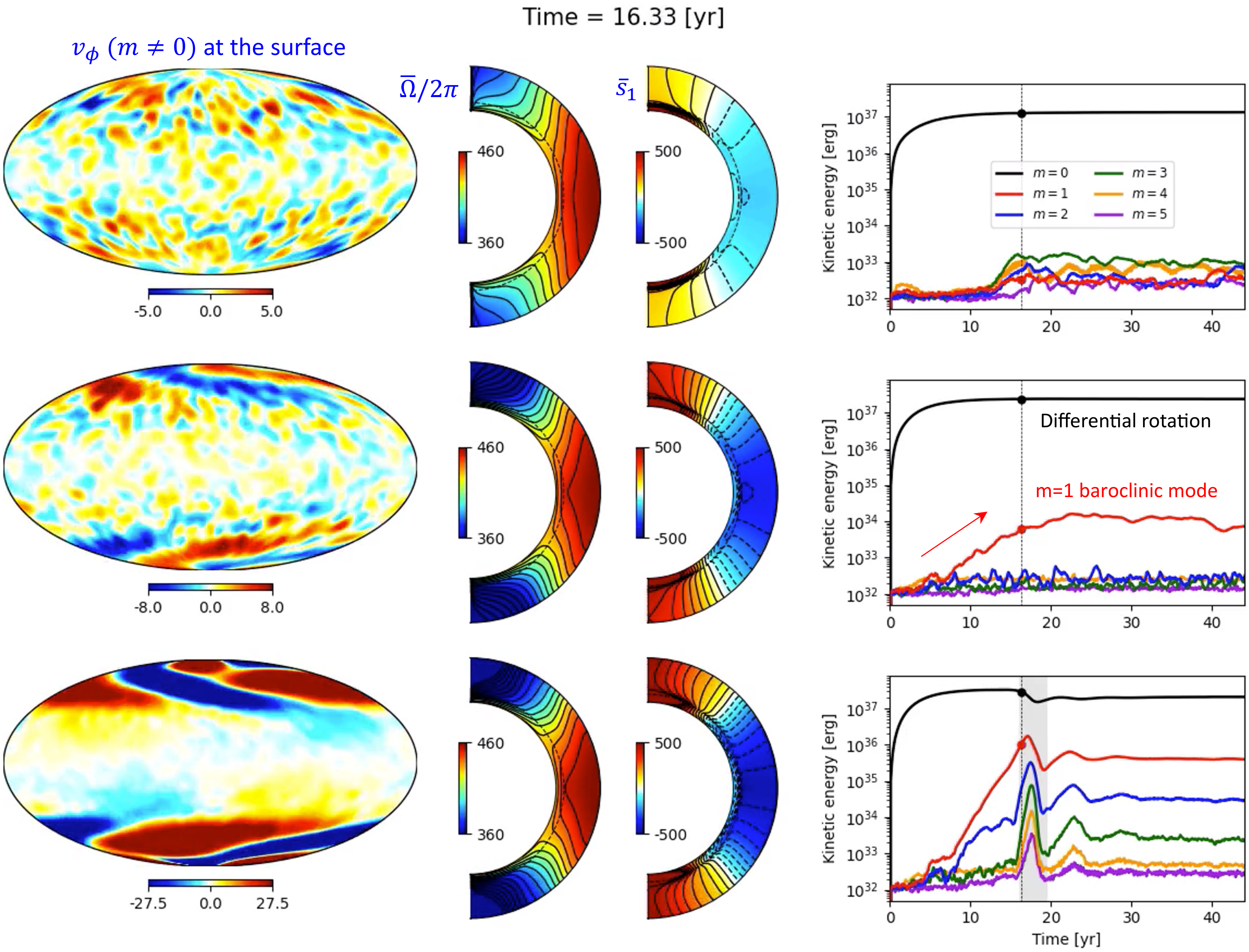

Nonlinear Results : Temporal evolution

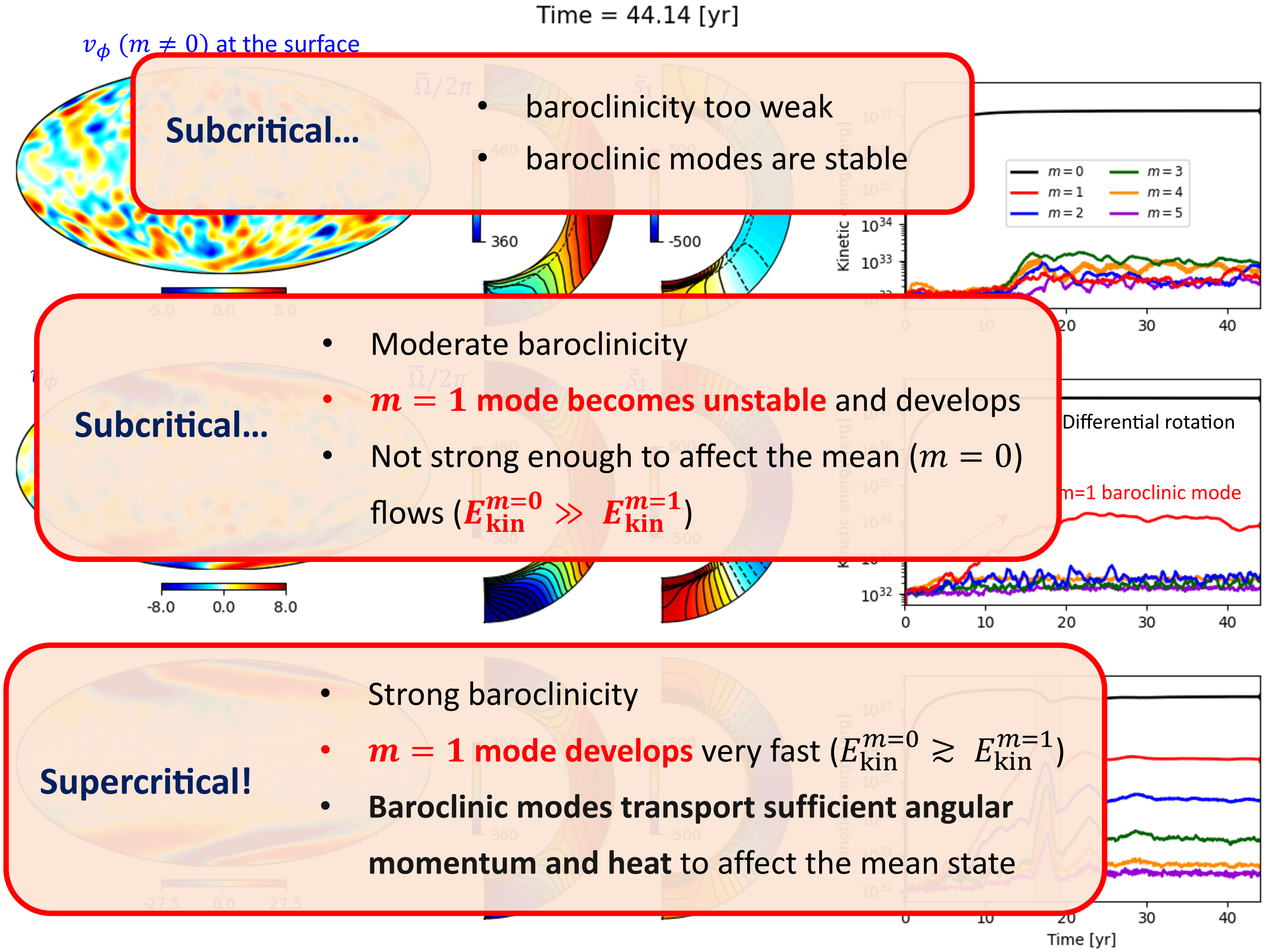

Case 1

$\delta_0 = -1\times10^{-5}$

Subcritical…

- baroclinicity too weak
- baroclinic modes are stable

Case 2

$\delta_0 = -2\times10^{-5}$

Subcritical…

- Moderate baroclinicity
- **$m = 1$ mode becomes unstable** and develops
- Not strong enough to affect the mean $(m = 0)$ flows $(E_{\text{kin}}^{m=0} \gg E_{\text{kin}}^{m=1})$

Case 3

$\delta_0 = -4\times10^{-5}$

Supercritical!

- Strong baroclinicity
- **$m = 1$ mode develops** very fast $(E_{\text{kin}}^{m=0} \gtrsim E_{\text{kin}}^{m=1})$
- **Baroclinic modes transport sufficient angular momentum and heat** to affect the mean state

Comparison : Observation vs. Simulation

Observation (SG tracking)

Simulation (Case 3)

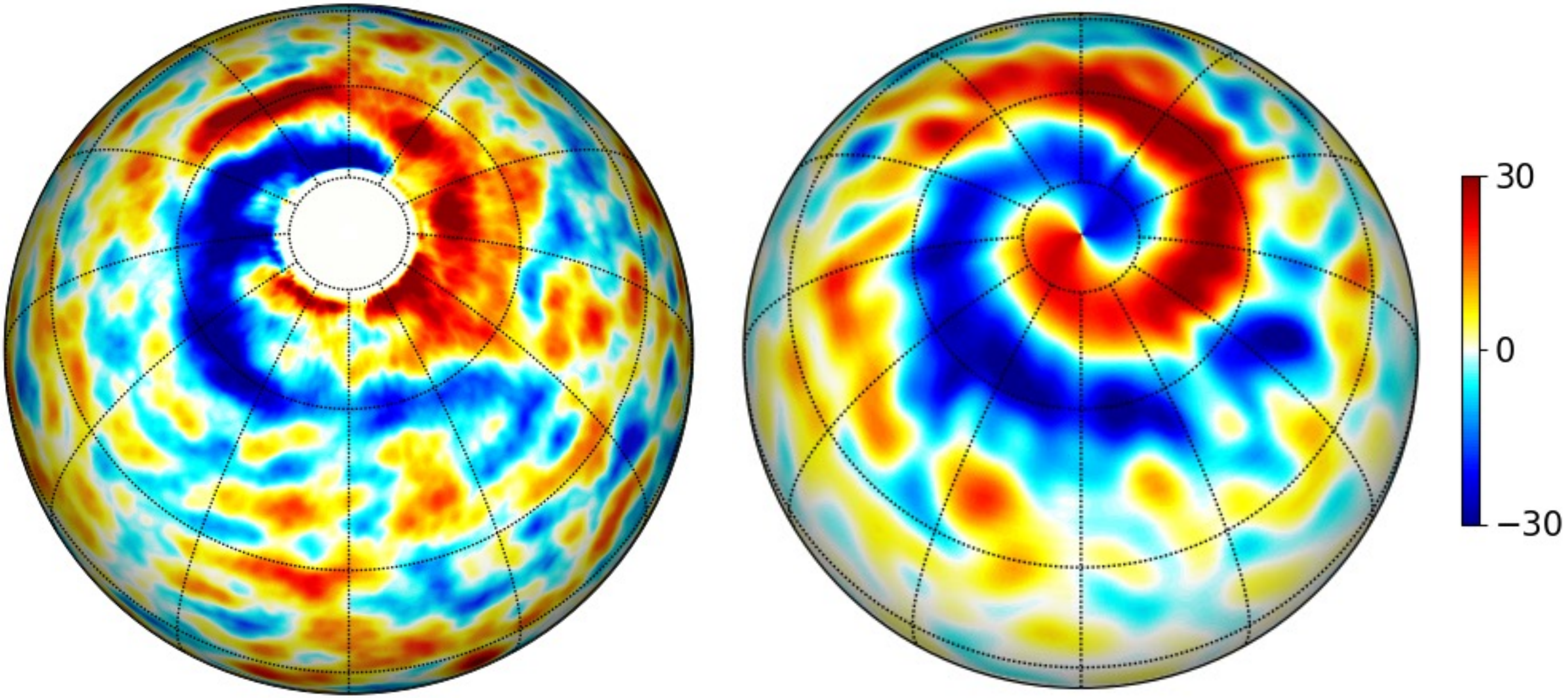

Data provided by Hathaway & Upton (2020)

Nonlinear Results II : Power spectrum and eigenfunctions

- The power ridge agree well with the dispersion relation of the observed high-latitude inertial modes
- Eigenfunctions are extracted using the singular-value decomposition (SVD)
- The eigenfunctions show a spiraling pattern similar to the observations
- **Baroclinic modes transport both angular momentum and heat equatorward**

Power spectrum near the surface averaged over high-latitudes

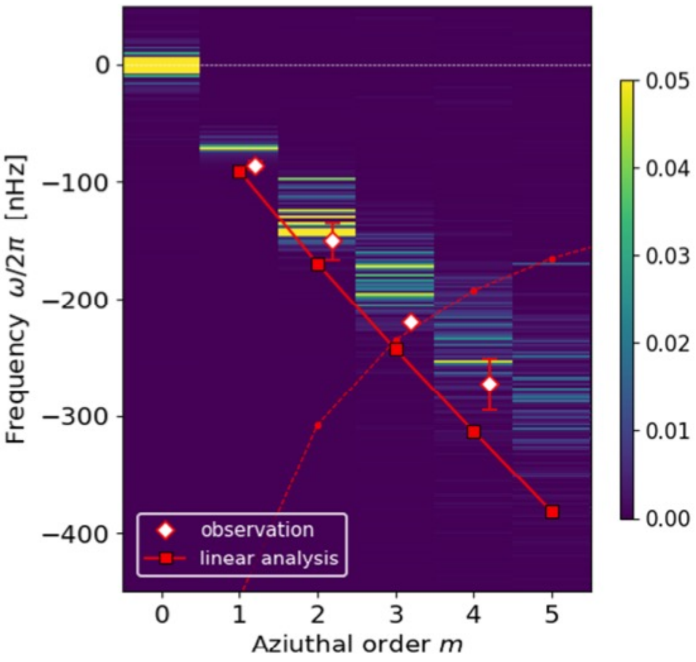

Extracted eigenfunctions at $m = 1$

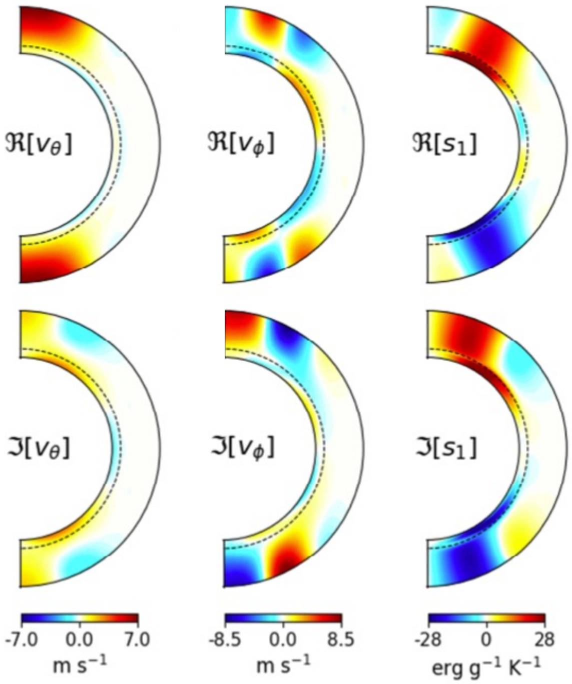

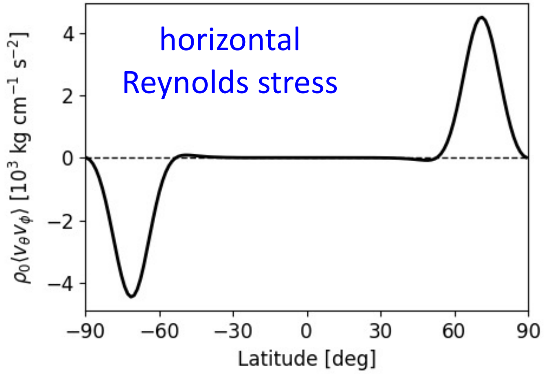

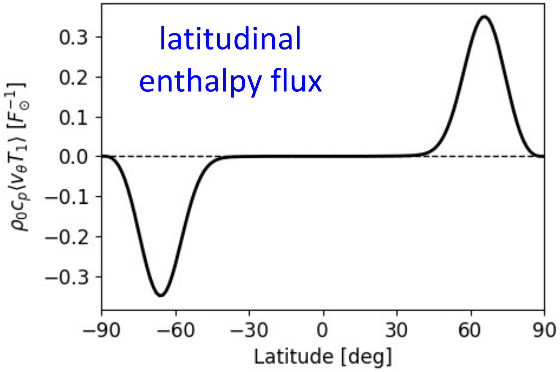

Nonlinear Results II : Power spectrum and eigenfunctions

- The power ridge agree well with the dispersion relation of the observed high-latitude inertial modes
- Eigenfunctions are extracted using the singular-value decomposition (SVD)
- The eigenfunctions show a spiraling pattern similar to the observations
- **Baroclinic modes transport both angular momentum and heat equatorward**

Baroclinic instability can be considered a mechanism that modulates the amplitude of the baroclinicity in the convection zone, and thus, controls the amplitude of the differential rotation in the Sun

Power spectrum averaged over high-latitudes

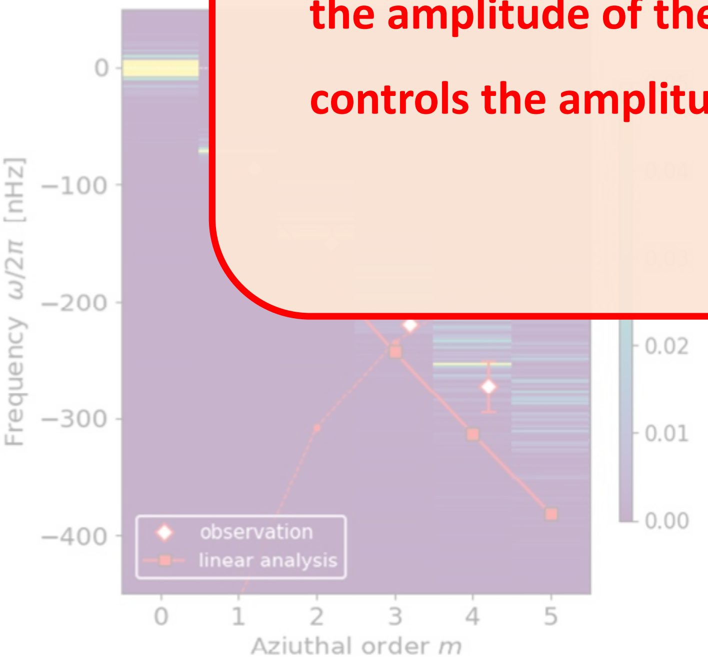

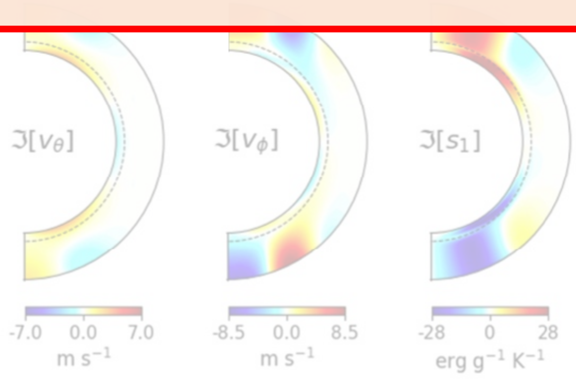

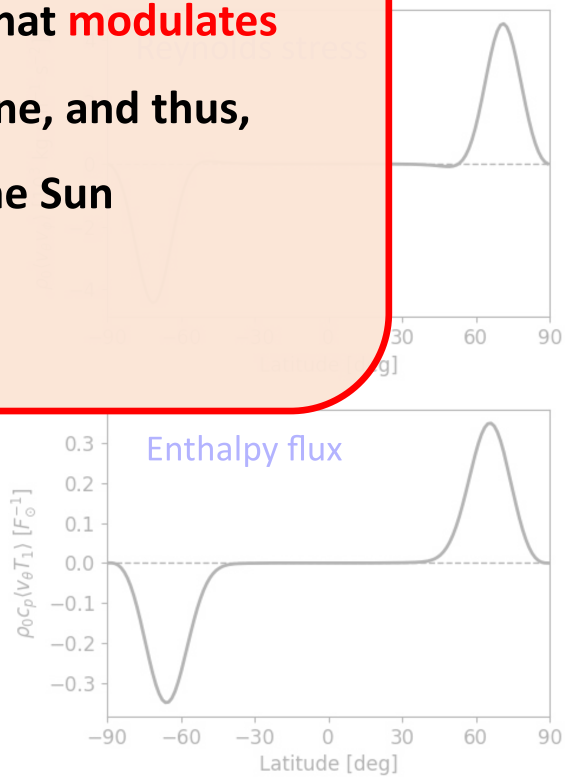

The role of magnetic fields : Motivation & Model

- Observations imply that the amplitude of high-latitude inertial modes change over the solar cycle

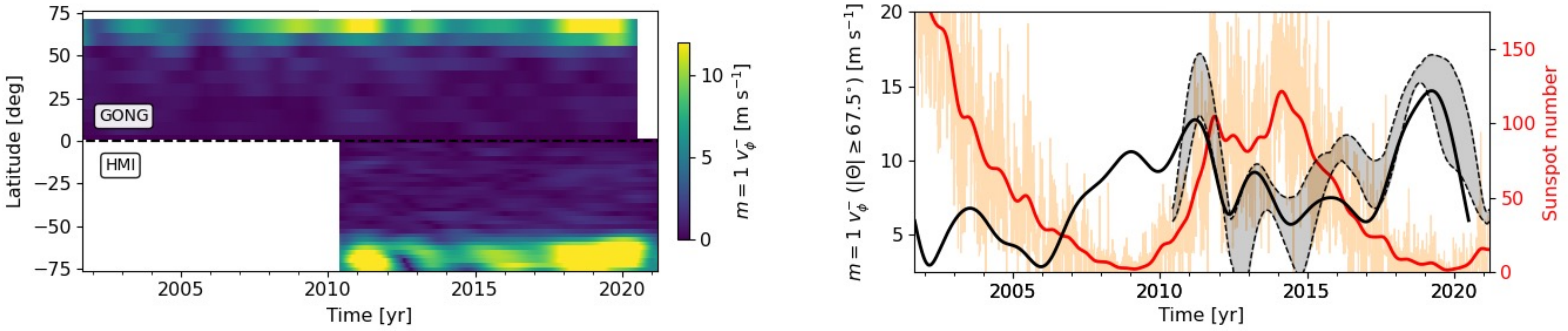

Courtesy of Z.C.Liang

- Our mean-field model is extended to MHD regime
- We add a strong toroidal field as an initial condition into the HD simulation Case 3
- Babcock-Leighton source is switched off (decaying)

motion: $$\rho_0 \frac{\partial \boldsymbol{v}}{\partial t} = [\ldots] + \frac{1}{4\pi}(\nabla \times \boldsymbol{B}) \times \boldsymbol{B},$$

entropy: $$\rho_0 T_0 \frac{\partial s_1}{\partial t} = [\ldots] + \frac{\eta}{4\pi}|\nabla \times \boldsymbol{B}|^2.$$

induction: $$\frac{\partial \boldsymbol{B}}{\partial t} = \nabla \times (\boldsymbol{v} \times \boldsymbol{B} + \cancel{\mathcal{E}_{\mathrm{BL}}} - \eta \nabla \times \boldsymbol{B}),$$

Bekki et al. 2021c (to be submitted)

MHD Results : Suppression effects by magnetic fields

- We numerically demonstrate that magnetic field has a suppressing effect for baroclinic instability [Gilman 2017]

- when $\boldsymbol{B}$ is added (strong), baroclinic modes are suppressed ⇨ $\Delta\Omega$ and Δs_1 are enhanced
- when $\boldsymbol{B}$ decays away, baroclinic modes become prominent ⇨ $\Delta\Omega$ and Δs_1 are suppressed

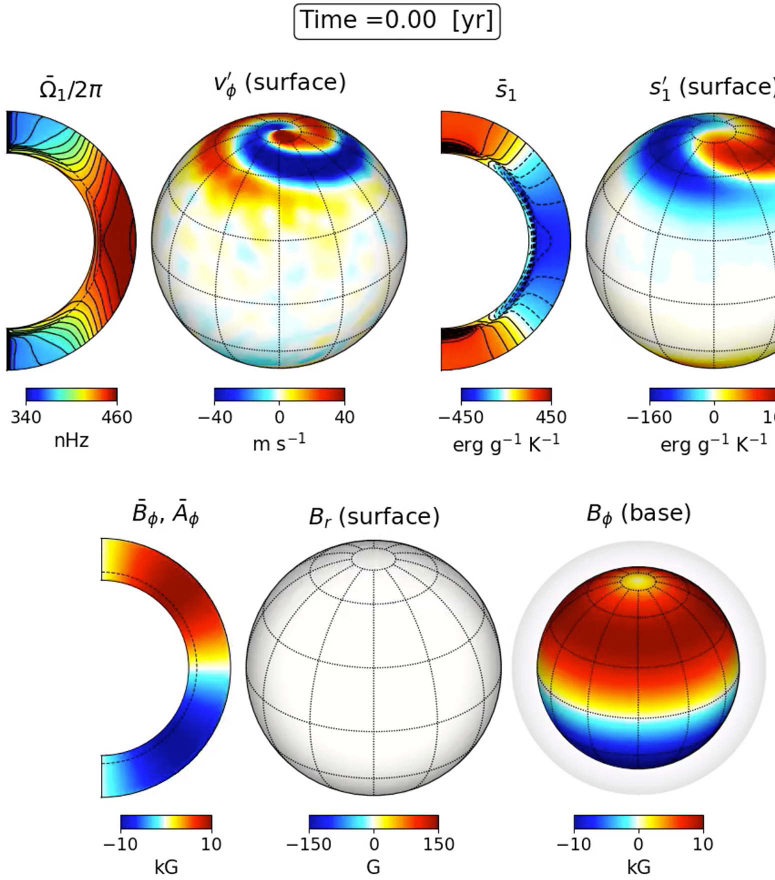

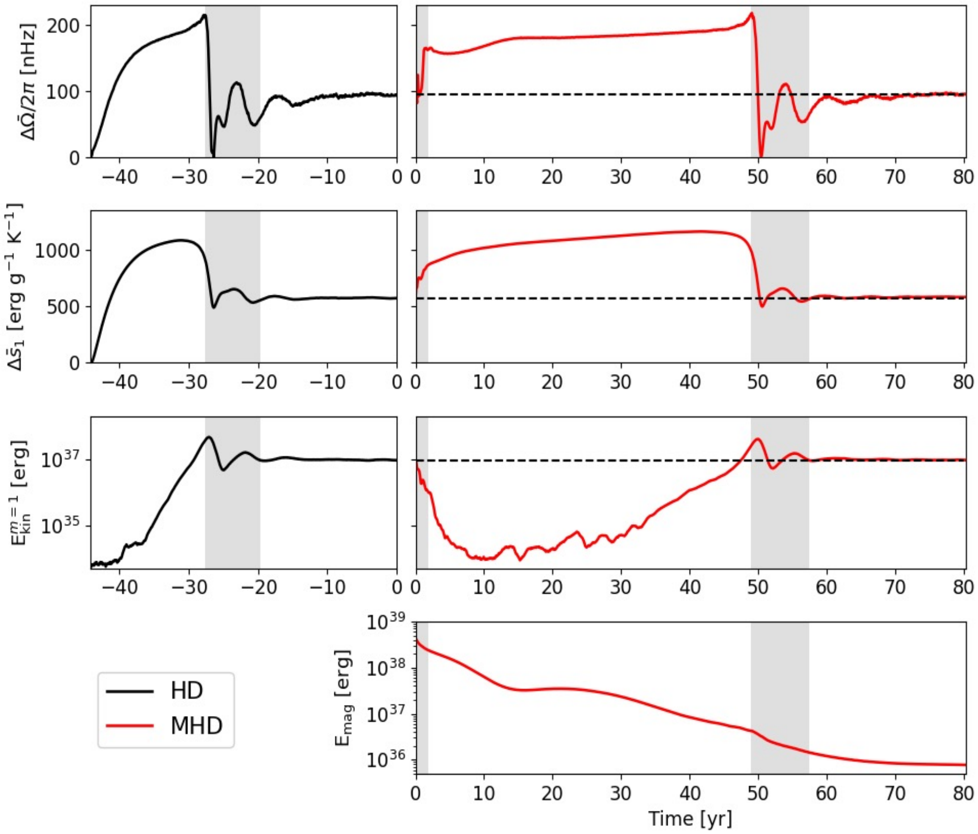

MHD Results : Cyclic Dynamo Simulation

- Babcock-Leighton source term is now switched on (**dynamo becomes cyclic**)
- Amplitude of the **high-latitude baroclinic modes oscillates along with the magnetic cycle**

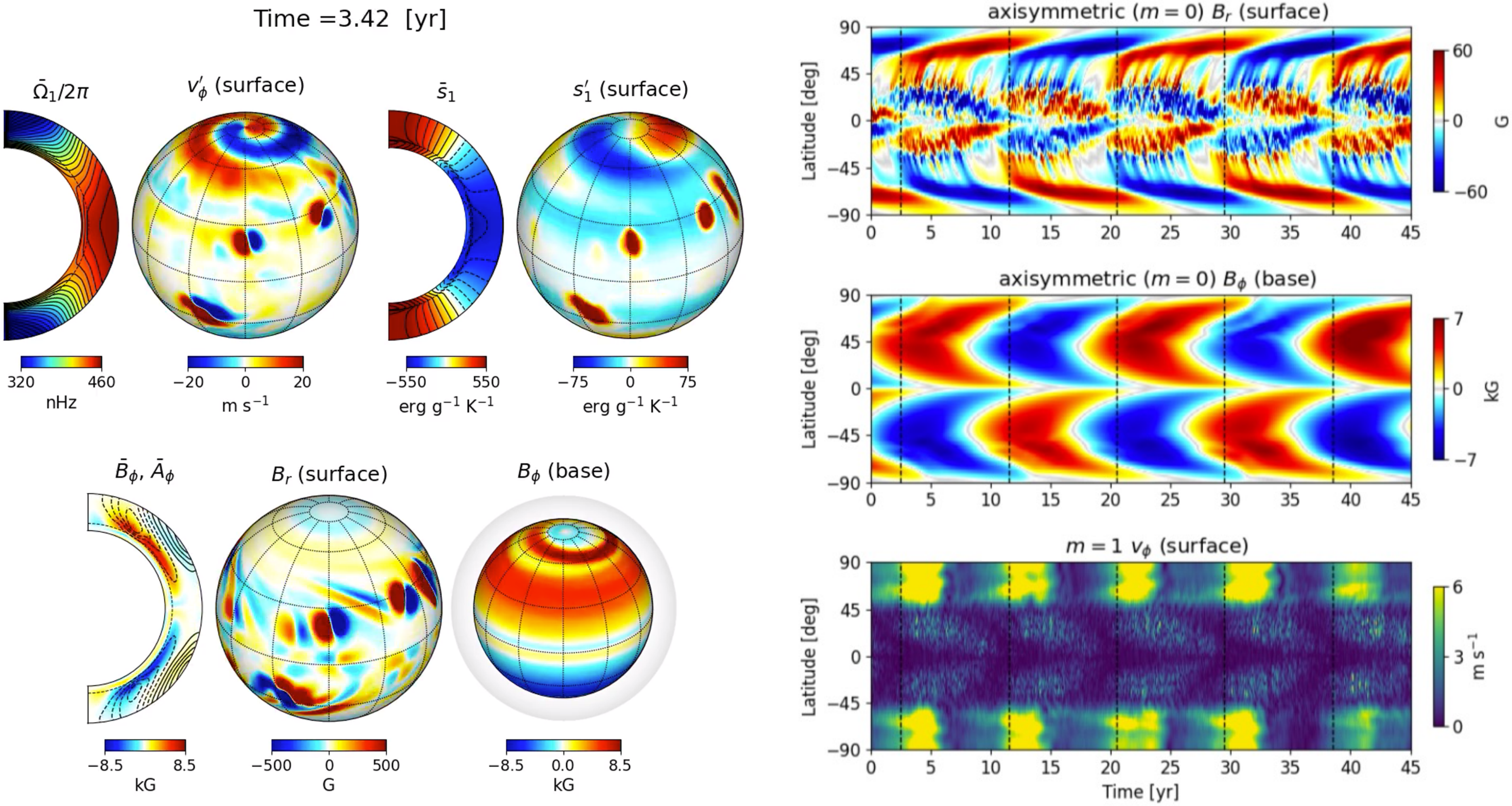

MHD Results : Cyclic Dynamo Simulation

- Babcock-Leighton source term is now switched on (**dynamo becomes cyclic**)
- Amplitude of the **high-latitude baroclinic modes oscillates along with the magnetic cycle**

- High-latitude baroclinic modes are strong (weak) during the rise (fall) of the magnetic activity cycle
- Accordingly, the **horizontal Reynolds stress and latitudinal heat flux are modulated with the activity cycle**

High-latitude power spectrum at $m = 1$

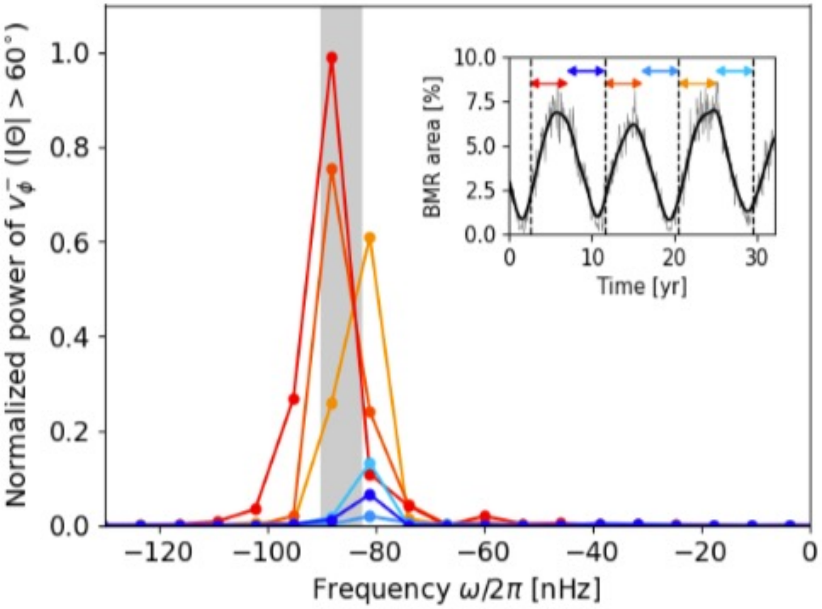

Horizontal Reynolds stress

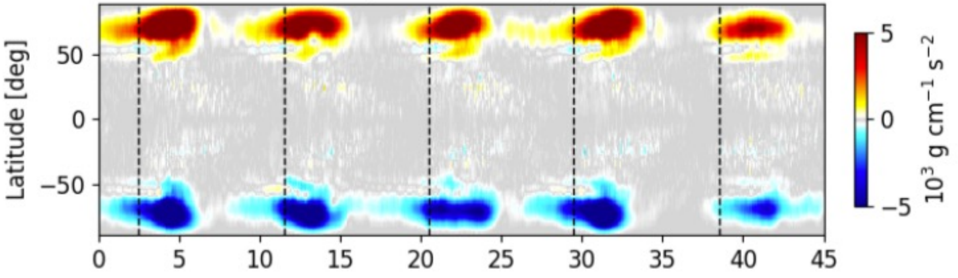

Latitudinal heat flux

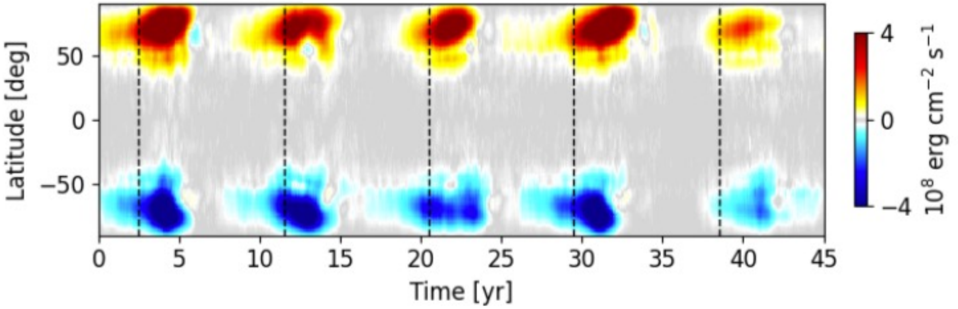

Summary

- **Recent interesting observations of inertial modes in the Sun** [Gizon et al., 2021]
  - Robust observations of the equatorial Rossby waves (r-modes) and high-latitude flow spirals
  - Thermal Rossby waves (that are repeatedly predicted in simulations) are NOT observed on the Sun
- **Mode coupling between r-modes and thermal Rossby waves**
  - Found both in the linear analysis and nonlinear convection simulations
  - Owing to this mode mixing, r-modes can partially transport the energy and angular momentum
- **Baroclinic instability in the Sun**
  - Quite ubiquitous in the Earth's atmosphere. Likely occur in the Sun's convection zone as well
  - The observed high-latitude flow properties can be well explained by baroclinic Rossby waves
  - Close interaction with the solar dynamo-generated magnetic fields

_ _

- Bekki et al., "Solar equatorial Rossby modes in a rotating convection simulation" (to be submitted to A&A)
- Bekki et al., "Linear model of global-scale inertial modes in the Sun's convection zone" (to be submitted to A&A)
- Bekki and Cameron., "3D MHD mean-field simulation of solar Babcock-Leighton dynamo" (to be submitted to A&A Letters)
- Bekki et al., "Baroclinic origin of the Sun's m=1 high-latitude inertial mode" (to be submitted to A&A)
- Bekki et al., "Solar cycle dependence of baroclinically-driven high-latitude inertial modes" (in prep)

Supplementary

Potential vorticity and β-effects

- Ignoring dissipation, Lorentz force, and radiative heating, the potential vorticity Π is materially conserved

$$\frac{D\Pi}{Dt} = 0, \quad \text{with} \quad \Pi = \frac{(\zeta + 2\Omega_0) \cdot \nabla S}{\rho}, \quad \text{where} \quad \zeta = \nabla \times v \quad \text{is a fluid vorticity}$$

- If the spherical surface is isentropic to a good approximation,

$$\frac{D}{Dt}(\zeta_r + 2\Omega_0 \sin\theta) = 0,$$

In the Eulerian form, $\frac{\partial \zeta_r}{\partial t} = \beta_r v_\theta + [\ldots v_r \text{ terms}\ldots]$,

where $\beta_r = \frac{2\Omega_0 \sin\theta}{r}$, is the planetary β-effect

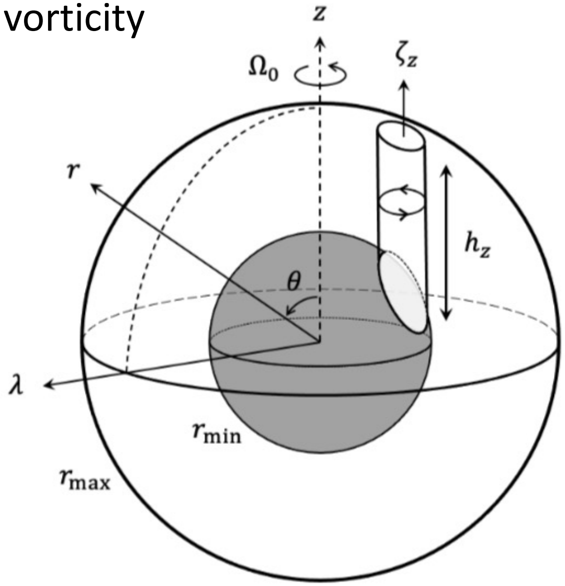

- If the xy-plane can be approximated to be isentropic,

$$\frac{D}{Dt}\left(\frac{\zeta_z + 2\Omega_0}{\rho}\right) = 0.$$

In the Eulerian form, $\frac{\partial \zeta_z}{\partial t} = (\beta_c + \beta_t)v_\lambda + [\ldots]$,

where $\beta_c = 2\Omega_0 \frac{d\ln\rho}{d\lambda} = -\frac{2\Omega_0}{H_\rho}$, is the compressional β-effect

and $\beta_t = 2\Omega_0 \frac{d\ln h_z}{d\lambda}$, is the topographic β-effect

$$h_z = \begin{cases} \sqrt{r_{\max}^2 - \lambda^2} - \sqrt{r_{\min}^2 - \lambda^2}, & (0 < \lambda < r_{\min}) \\ 2\sqrt{r_{\max}^2 - \lambda^2}, & (r_{\min} < \lambda < r_{\max}) \end{cases}$$

Here, we used the integrated equation of continuity $\nabla \cdot (h_z \rho v) = 0.$

Compressional β-effect vs. Topographic β-effect

For the solar internal model S (Jorgen Christensen-Dalsgaard 1996)

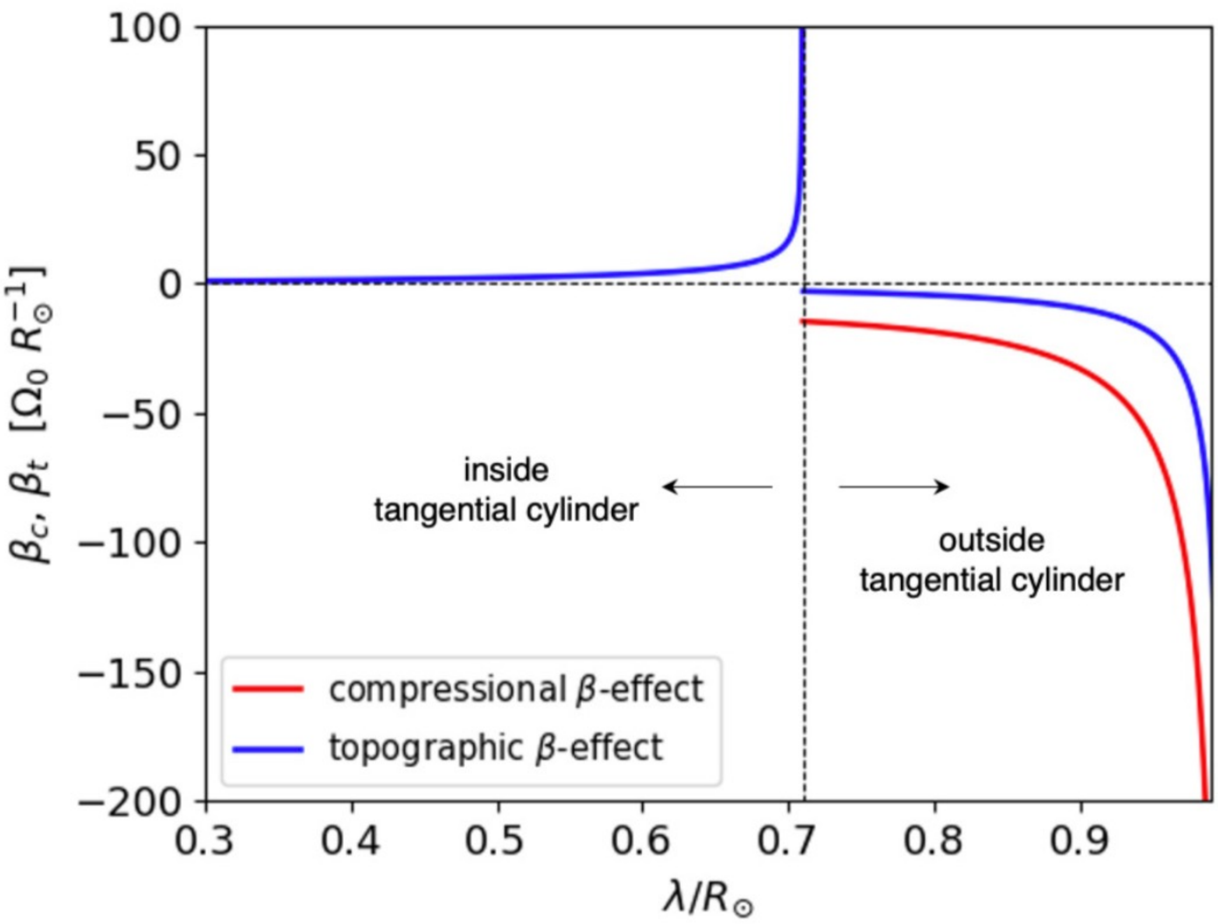

Dispersion relations of the Major Rossby waves in the Sun

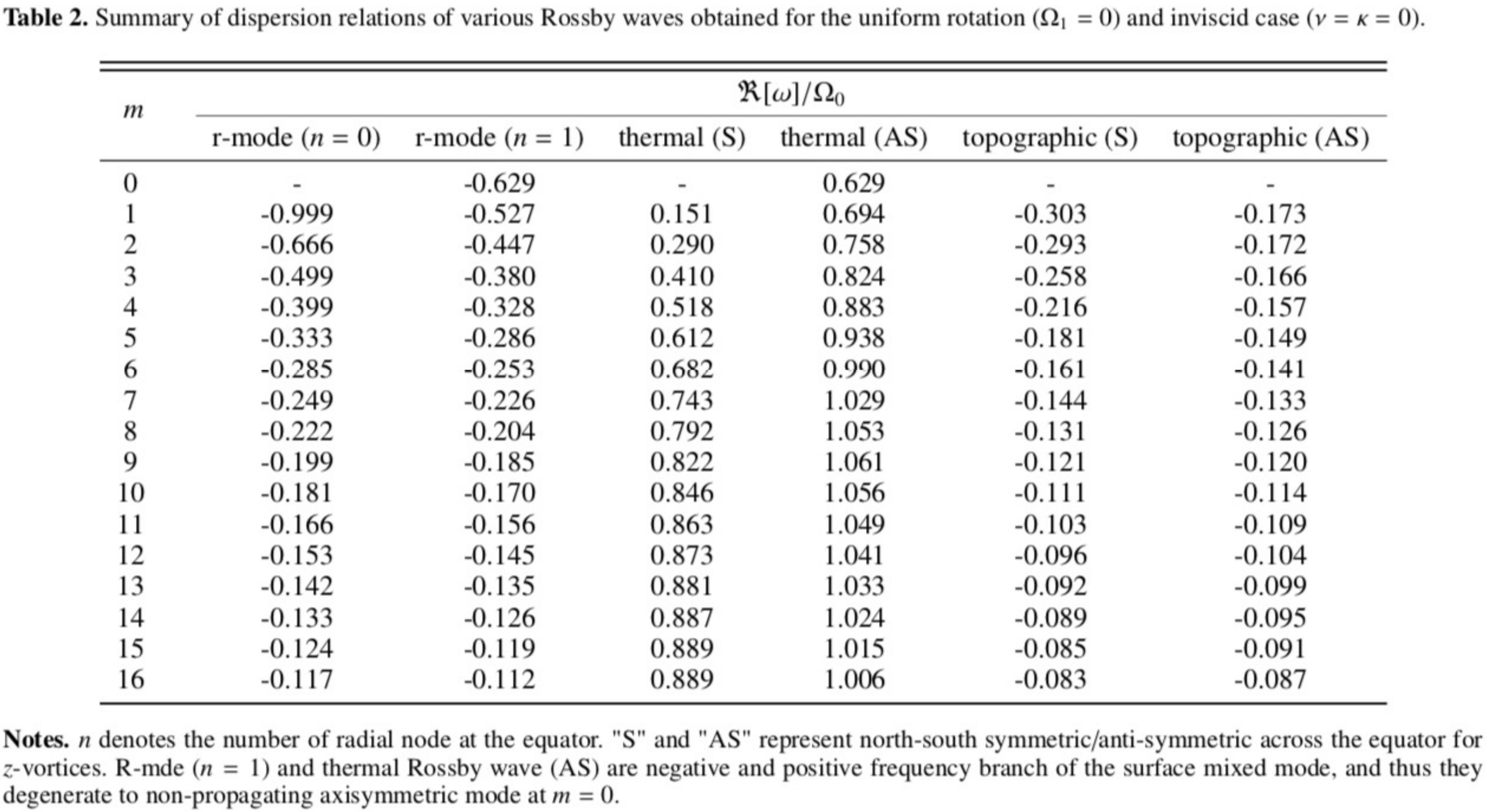

Table 2. Summary of dispersion relations of various Rossby waves obtained for the uniform rotation ($\Omega_1 = 0$) and inviscid case ($\nu = \kappa = 0$).

m	$\Re[\omega]/\Omega_0$					
	r-mode ($n = 0$)	r-mode ($n = 1$)	thermal (S)	thermal (AS)	topographic (S)	topographic (AS)
0	-	-0.629	-	0.629	-	-
1	-0.999	-0.527	0.151	0.694	-0.303	-0.173
2	-0.666	-0.447	0.290	0.758	-0.293	-0.172
3	-0.499	-0.380	0.410	0.824	-0.258	-0.166
4	-0.399	-0.328	0.518	0.883	-0.216	-0.157
5	-0.333	-0.286	0.612	0.938	-0.181	-0.149
6	-0.285	-0.253	0.682	0.990	-0.161	-0.141
7	-0.249	-0.226	0.743	1.029	-0.144	-0.133
8	-0.222	-0.204	0.792	1.053	-0.131	-0.126
9	-0.199	-0.185	0.822	1.061	-0.121	-0.120
10	-0.181	-0.170	0.846	1.056	-0.111	-0.114
11	-0.166	-0.156	0.863	1.049	-0.103	-0.109
12	-0.153	-0.145	0.873	1.041	-0.096	-0.104
13	-0.142	-0.135	0.881	1.033	-0.092	-0.099
14	-0.133	-0.126	0.887	1.024	-0.089	-0.095
15	-0.124	-0.119	0.889	1.015	-0.085	-0.091
16	-0.117	-0.112	0.889	1.006	-0.083	-0.087

Notes. n denotes the number of radial node at the equator. "S" and "AS" represent north-south symmetric/anti-symmetric across the equator for z-vortices. R-mde ($n = 1$) and thermal Rossby wave (AS) are negative and positive frequency branch of the surface mixed mode, and thus they degenerate to non-propagating axisymmetric mode at $m = 0$.

Angular momentum transport by r-modes

$$\nabla \cdot (\boldsymbol{F}_{\mathrm{RS}} + \boldsymbol{F}_{\mathrm{MC}} + \boldsymbol{F}_{\mathrm{VD}}) = 0, \quad \left\{ \begin{aligned} \boldsymbol{F}_{\mathrm{RS}} &= \rho_0 r \sin\theta \langle \boldsymbol{v}_m v_\phi \rangle, \\ \boldsymbol{F}_{\mathrm{MC}} &= \rho_0 r^2 \sin^2\theta \boldsymbol{v}_m \Omega, \\ \boldsymbol{F}_{\mathrm{VD}} &= -\rho_0 \nu r^2 \sin^2\theta \nabla\Omega, \end{aligned} \right.$$

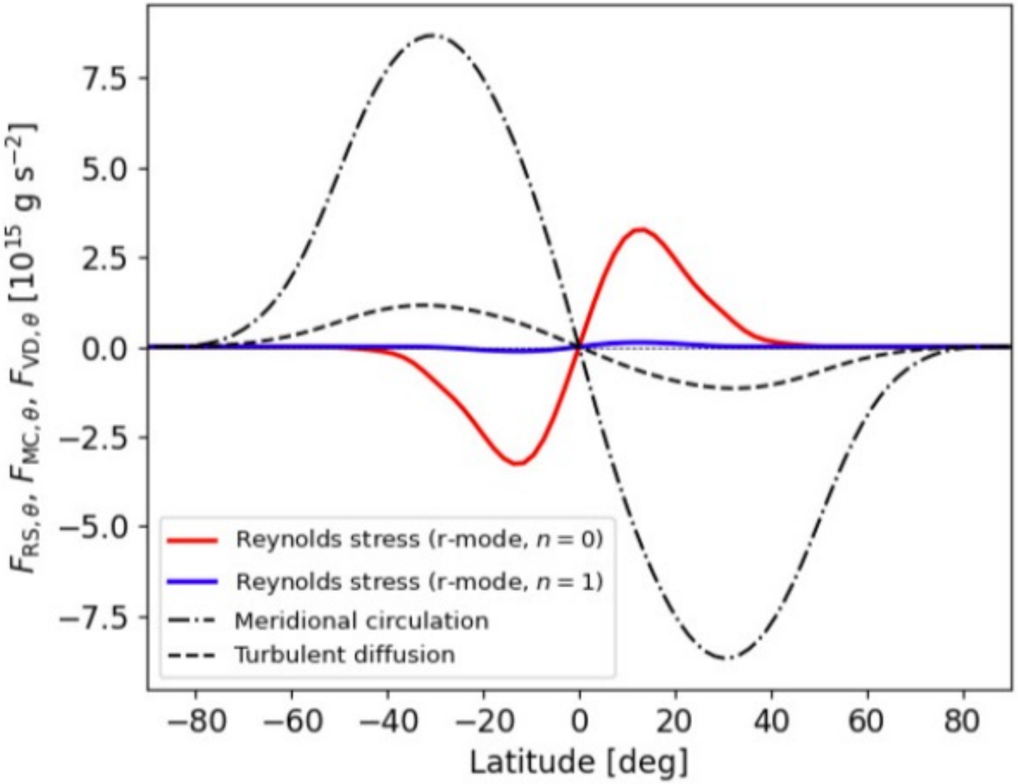

Effects of Turbulent Diffusivities on r-modes

Typical oscillation period of Rossby waves at azimuthal order m is given by

$$\tau_{\rm Ro} = \left|\frac{2\pi}{\omega_{\rm Ro}}\right|, \quad \text{where} \quad \omega_{\rm Ro} = -\frac{2\Omega_0}{m+1}.$$

Typical diffusive time scale is $\tau_{\rm diff} = \frac{l_m^2}{\nu}, \quad \text{with} \quad l_m = \frac{R_\odot}{m},$

For a given diffusivity, the critical azimuthal order can be defined $m_{\rm crit} = \left(\frac{R_\odot \Omega_0}{\pi\nu}\right)^{1/3}.$

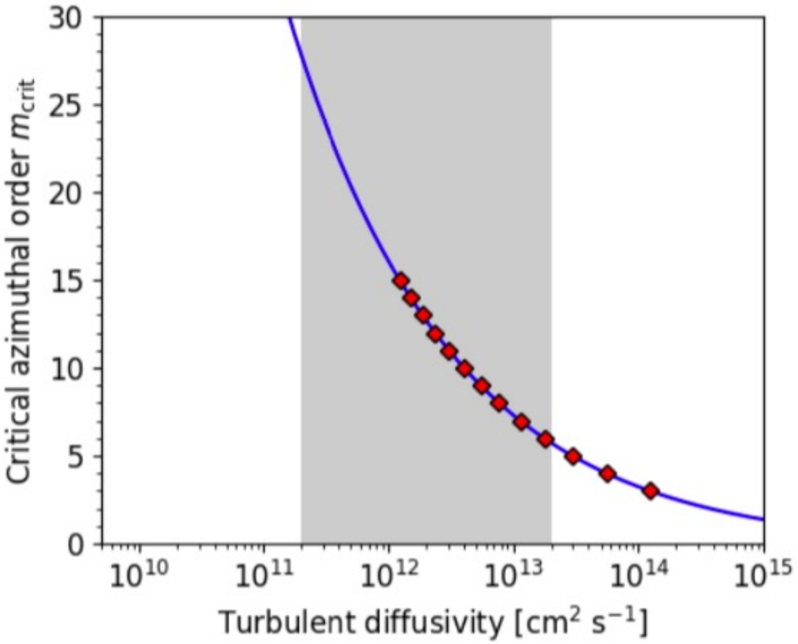

Thermal Rossby waves become convectively-unstable

- Thermal Rossby waves become unstable when the background stratification is changed towards superadiabatic ($\delta > 0$)
- Propagation frequencies decrease (increase) when $\delta > 0$ ($\delta < 0$)

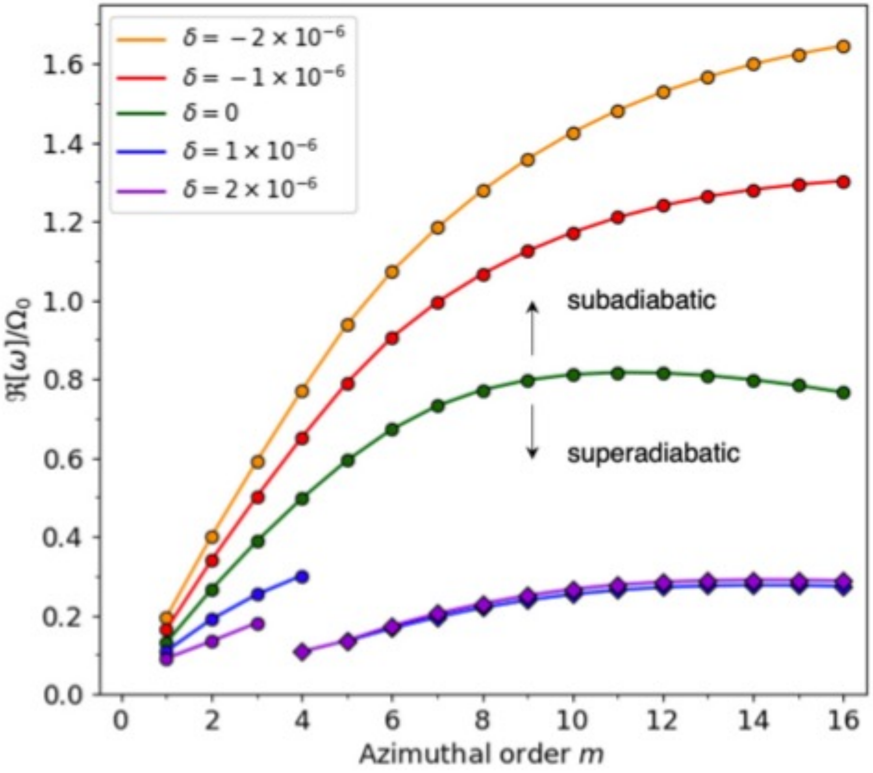

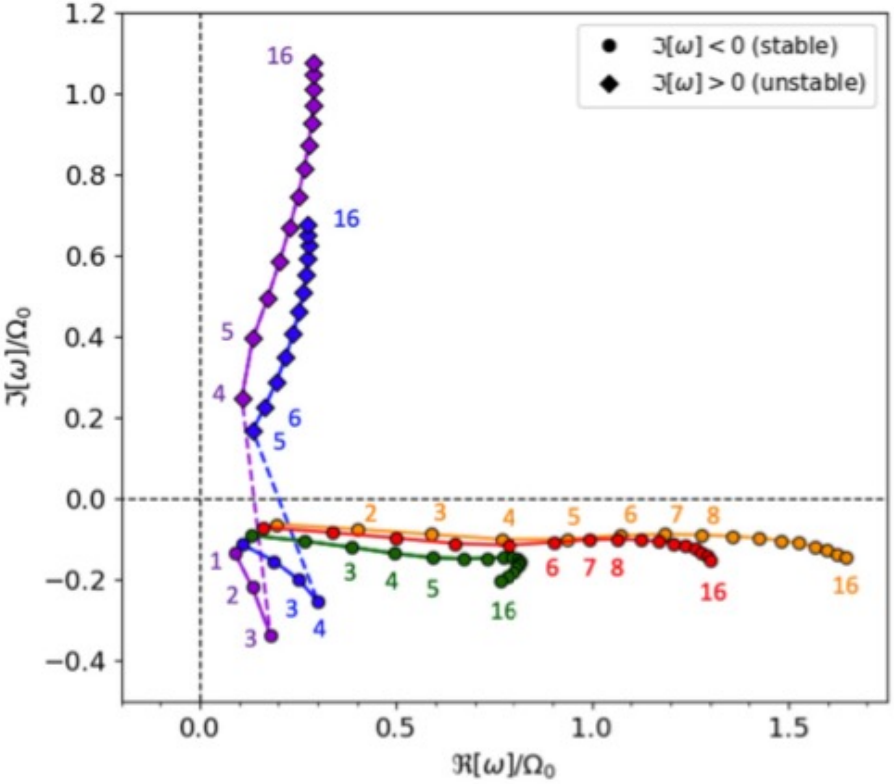

Transport properties by thermal Rossby waves

- Propagation frequencies decrease (increase) when $\delta > 0$ ($\delta < 0$)

⇦ depends on the way it couples with g-modes (additional restoring force)

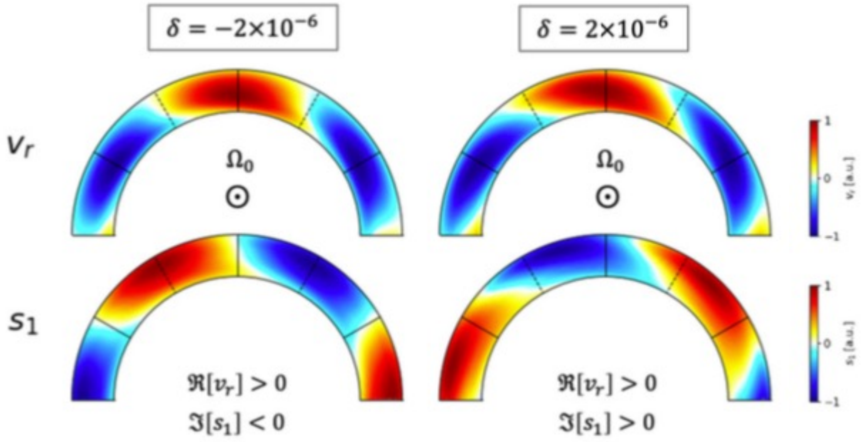

- When the background is superadiabatic ($\delta > 0$), thermal Rossby waves transport heat and angular momentum upwards, and equatorwards

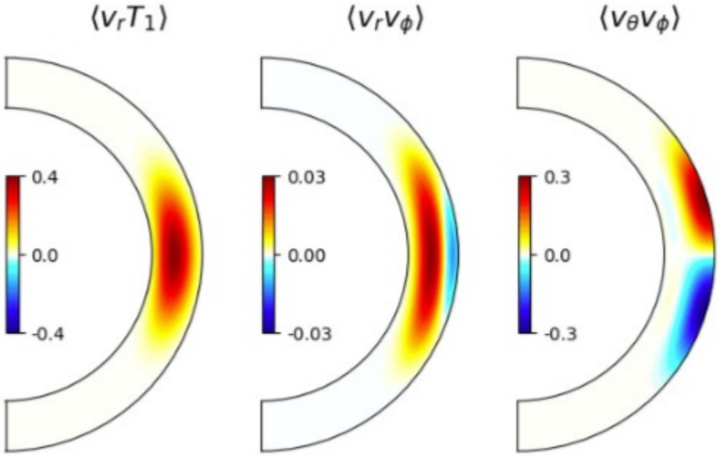

Power spectra comparison : Observation vs. Simulation

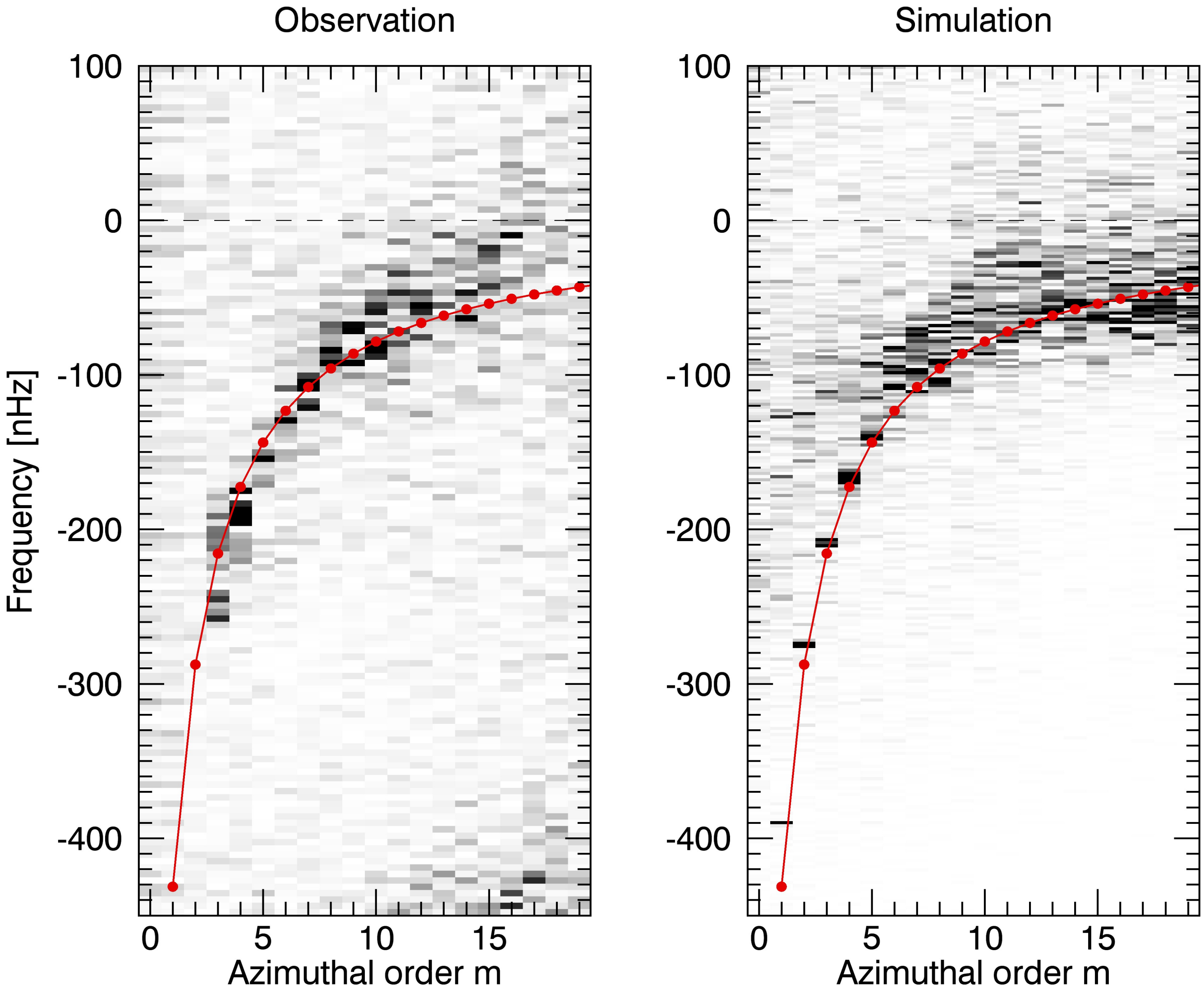

Singular Value Decomposition

Let $q(r,\theta,\phi;t)$ be a variable that characterizes the mode of interest.

FFT in time and longitude, we have $\tilde{q}(r,\theta;m;\omega)$

At fixed m, we compute the equatorial spectrum $\tilde{q}_{eq}(r;\omega)$

Depending on the mode of interest, we may limit (r,θ) domain to be focused
$\tilde{q}_{\rm eq}(r \in [r_1, r_2], \omega \in [\omega_1, \omega_2])$ so that the prominent power peak exists inside the domain.

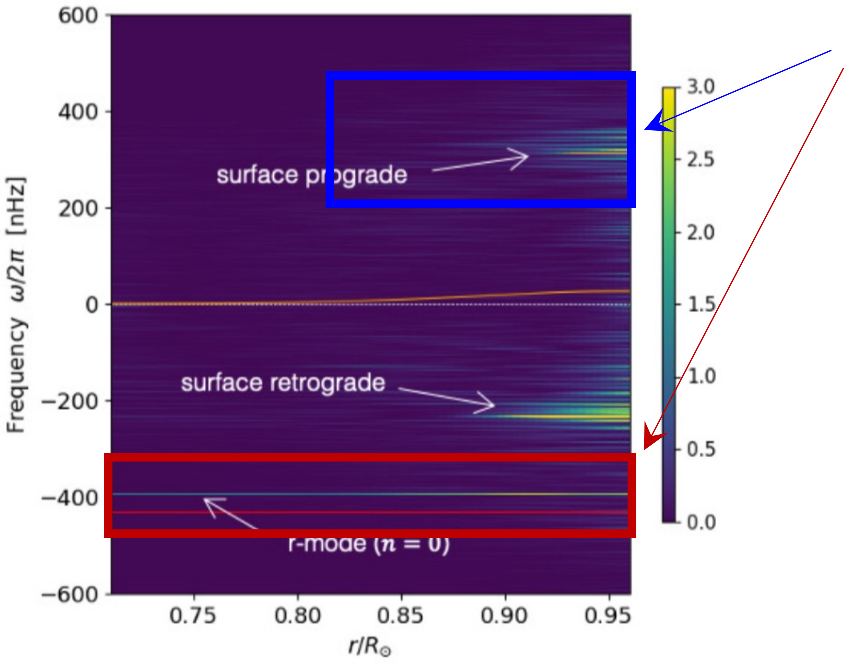

Applying SVD, the spectrum is decomposed as

$$\tilde{q}_{\rm eq}(r', \omega') = \sum_k \sigma_k U_k(r') V_k^*(\omega'),$$

Only keeping the 1st singular value σ_0 gives a desired decomposition of $\tilde{q}_{\rm eq}(r', \omega')$ into one radii U_0 and one frequency function V_0

Eigenfunctions of an arbitrary variable ψ are calculated as,

$$\psi_{\rm eigen}(r, \theta) = \sum_{\omega'=\omega_1}^{\omega_2} \psi(r, \theta; \omega') V_0(\omega').$$

Numerical methods : Babcock-Leighton dynamo code I

mass:

$$\frac{\partial \rho_1}{\partial t} = -\frac{1}{\xi^2}\nabla\cdot(\rho_0 \boldsymbol{v}),$$

motion:

$$\frac{\partial \boldsymbol{v}}{\partial t} = -\boldsymbol{v}\cdot\nabla\boldsymbol{v} - \frac{\nabla p_1}{\rho_0} - \frac{\rho_1}{\rho_0} g \boldsymbol{e}_r + 2\boldsymbol{v}\times\boldsymbol{\Omega_0} + \frac{1}{4\pi\rho_0}(\nabla\times\boldsymbol{B})\times\boldsymbol{B} + \frac{1}{\rho_0}\nabla\cdot\boldsymbol{\Pi},$$

induction:

$$\frac{\partial \boldsymbol{B}}{\partial t} = \nabla\times(\boldsymbol{v}\times\boldsymbol{B} + \boldsymbol{\mathcal{E}} - \eta\nabla\times\boldsymbol{B}),$$

entropy:

$$\frac{\partial s_1}{\partial t} = \boldsymbol{v}\cdot\nabla\boldsymbol{s_1} + c_{\mathrm{p}}\delta\frac{v_r}{H_p} + \frac{1}{\rho_0 T_0}\nabla\cdot(\rho_0 T_0 \kappa \nabla s_1) + \frac{1}{\rho_0 T_0}\left[(\boldsymbol{\Pi}\cdot\nabla)\cdot\boldsymbol{v} + \frac{\eta}{4\pi}|\nabla\times\boldsymbol{B}|^2\right],$$

- "Mean-field" MHD equations in a 3D full-spherical shell (**NOT azimuthal mean**)
- Small-scale convective angular momentum transport (**Λ-effect**) is parameterized [Kitchatinov & Rudiger 1995]

$$\Pi_{ik} = \rho_0\left[\nu_{\mathrm{vis}}\left(S_{ik} - \frac{2}{3}\delta_{ik}\nabla\cdot\boldsymbol{v}\right) + \nu_{\mathrm{lam}}\Lambda_{ik}\Omega_0\right]$$

- Convective energy transport is implicitly assumed
- Lower CZ is set weakly subadiabatic to achieve the thermal wind balance [Rempel 2005]

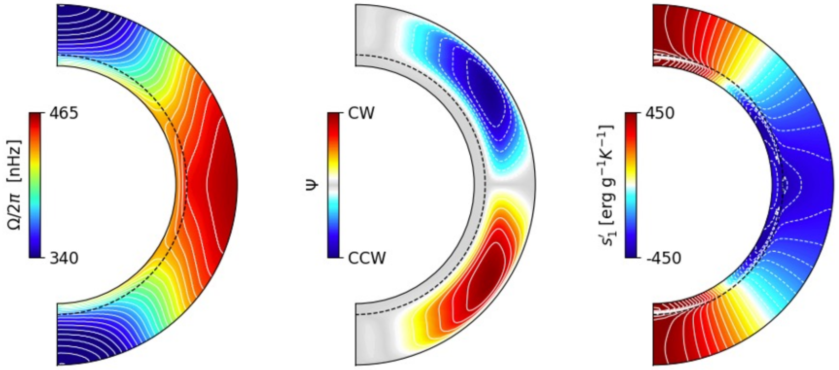

HD solver

Numerical methods : Babcock-Leighton dynamo code II

induction: $$\frac{\partial \boldsymbol{B}}{\partial t} = \nabla \times (\boldsymbol{v} \times \boldsymbol{B} + \boldsymbol{\mathcal{E}} - \eta \nabla \times \boldsymbol{B}),$$

Bipolar magnetic regions (BMRs) are produced instantaneously at the surface in response to the dynamo-generated toroidal field near the base of CZ

[step I] determine the location of BMR emergence (θ^*, ϕ^*) that satisfies the following condition

$$f_{\mathrm{eq}}(\theta^*) B_\phi(\theta^*, \phi^*)|_{r=r_{\mathrm{bcz}}} > B_{\mathrm{crit}} = 500\ \mathrm{G}$$

suppress high-latitude emergence

toroidal field near the base

threshold field strength for emergence

[step 2] electro-motiver force $\mathcal{E}$ is set proportional to $B_\phi(\theta^*, \phi^*)$

$$\begin{pmatrix} \mathcal{E}_\theta \\ \mathcal{E}_\phi \end{pmatrix} = \alpha_0 f_{\mathrm{sf}}(r, \theta, \phi) \begin{pmatrix} -\cos\psi^* \\ \sin\psi^* \end{pmatrix} B_\phi(\theta^*, \phi^*)|_{r=r_{\mathrm{bcz}}}$$

localized near the surface

Joy's law tilt: $\psi^* = 35^\circ \cos\theta^*$

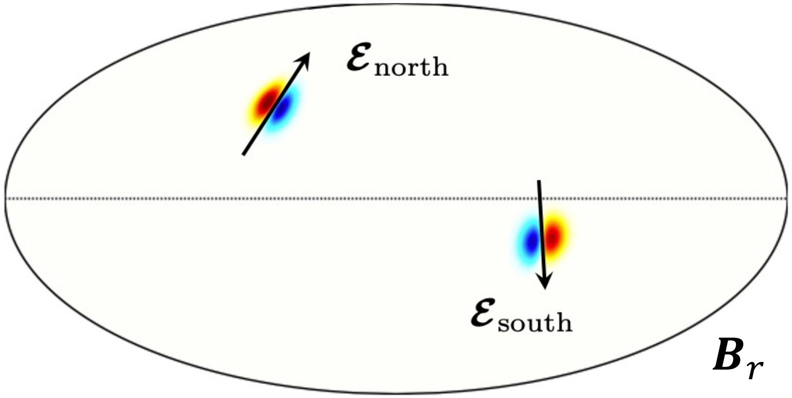

[step 3] frequency of BMR emergence is determined by the log-normal time-delay distriobution with $\Delta_s = t - t_s \gtrsim 10$ days

R-modes in the mean-field simulations

- Observations suggest that Rossby waves (r-modes) are importanat ingredients for large-scale dynamics [Loeptien et al. 2018]
- r-modes exist at roughly $3 \lesssim m \lesssim 15$ (possibly excited by **non-axisymmetric Lorentz force**)
- Extracted eigenfunction of v_θ peaks at the equator, changes its sign, and decays at higher latitudes [Proxauf et al. 2020]
- r-mode's eigenfunctions are strongly trapped in the equatorial region by the viscous critical layers [Gizon et al. 2020]

Power of v_θ near the surface

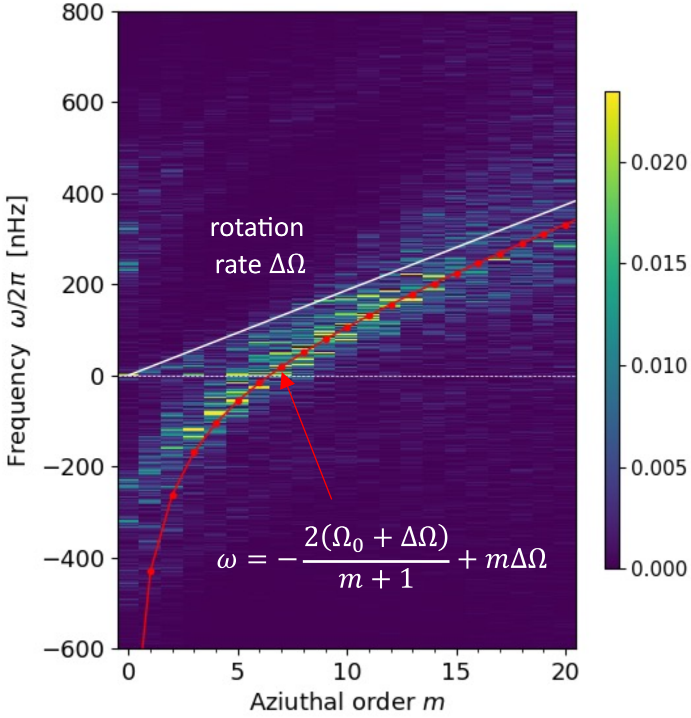

extracted eigenfunction at $m = 8$

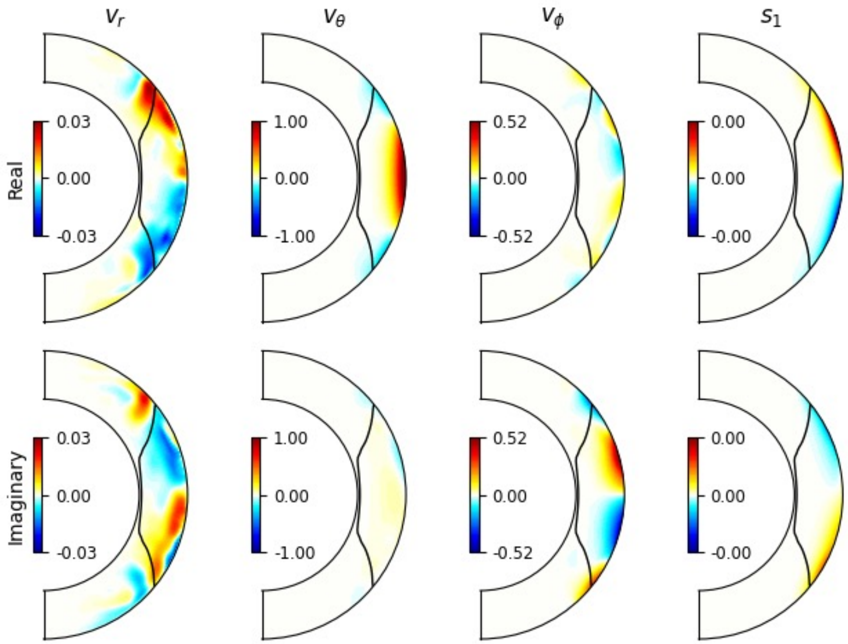

Physical Picture of Baroclinic instability

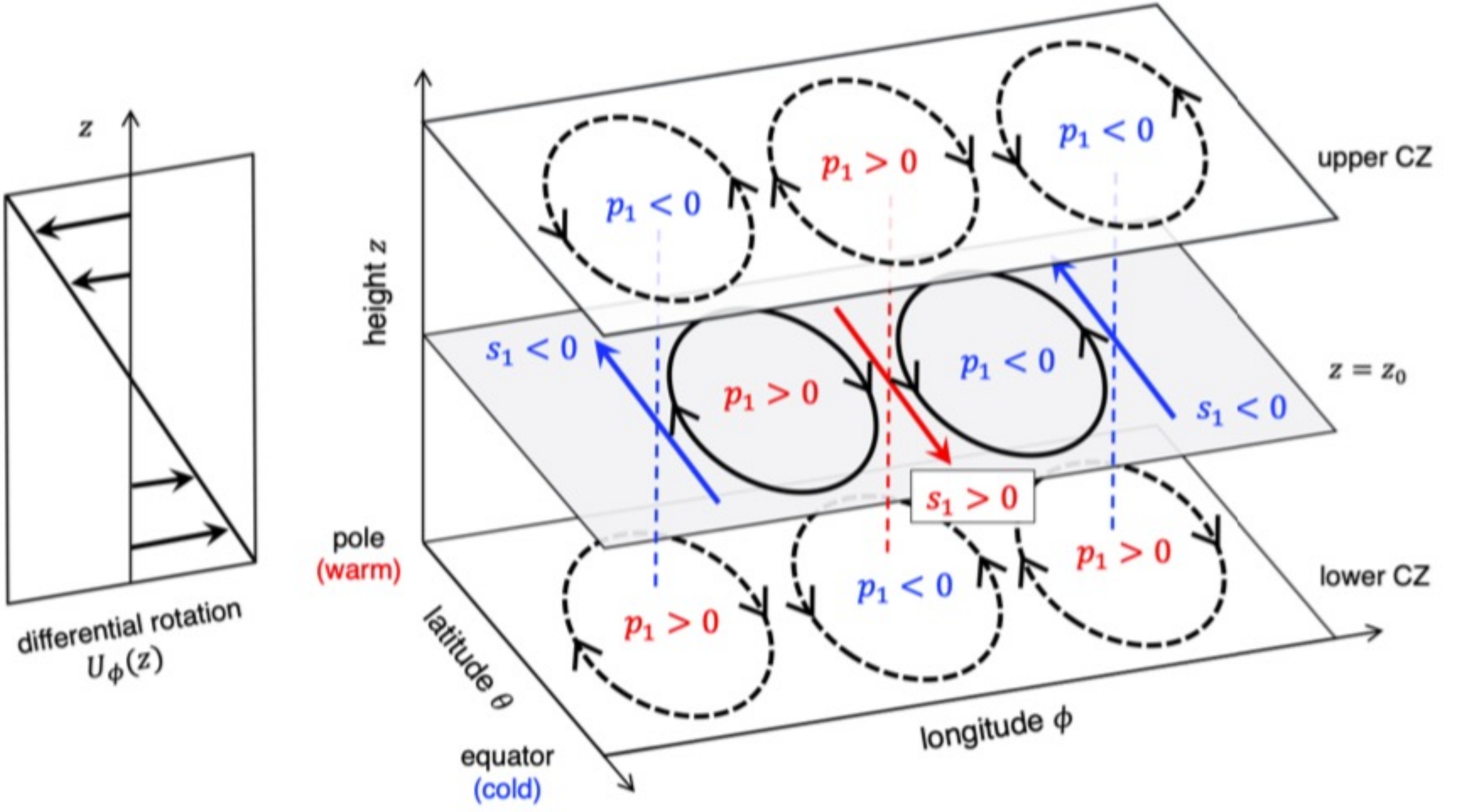

Numerical Simulation of Baroclinic instability

thermal wind balance
($t = 0$)

$$\frac{\partial v_x}{\partial z} < 0$$

$$\frac{\partial s_1}{\partial y} > 0$$